

A revised age-model for the Eocene deep-marine siliciclastic systems,

Aínsa Basin, Spanish Pyrenees

Blanca Cantalejo ^{1*}, Kevin T. Pickering ¹, Conall McNiocail ², Paul Bown ¹,

Kyrre Johansen ², Melissa Grant ²

¹ Department of Earth Sciences, University College London (UCL), Gower Street, London, WC1E 6BT, U.K.

² Department of Earth Sciences, University Oxford, South Parks Road, Oxford, OX1 3AN, U.K.

*Correspondence (ucfbca@ucl.ac.uk)

Keywords magnetostratigraphy, biostratigraphy, nannofossils, deep-marine, Middle Eocene, Aínsa Basin

Abstract

Using new palaeomagnetic and biostratigraphic data, we revise the age-model for the middle Eocene, deep-marine, Aínsa Basin (Spanish Pyrenees), a tectonically active basin formed at a convergent-plate margin. This new age model provides a framework for evaluating the depositional history and sediment accumulation rates. New integrated magneto- and biostratigraphy data identifies two normal and two reverse chrons of the geomagnetic polarity timescale (C21r, C21n, C20r, C20n) and place these Upper Hecho Group deposits in the middle Eocene (Lutetian). Nannofossil analysis identifies a biostratigraphic range from Subzone NP14b in the Gerbe System to Subzone NP15b at the top of the Aínsa System using key, age-diagnostic marker species such as *Blackites inflatus*, *Blackites piriformis* and *Coccolithus gigas*. We also present new nannofossil biostratigraphy from the Lower Hecho Group. This new Aínsa Basin chronostratigraphy enables inter-basinal correlations between the proximal fluvio-deltaic Tremp-Graus Basin and the more distal Jaca Basin, thereby providing a better understanding of the basin evolution.

A robust age-model is a prerequisite for understanding the interplay of tectonic, climatic and autocyclic processes in controlling stratigraphic architecture, and resolving source to sink

configurations in deep time (e.g., Cecil, 2003; Allen, 2008; Romans et al., 2016; Matengo and Haq, 2020).

Through the integration of new palaeomagnetic and biostratigraphic data, we refine the existing age model of Scotchman et al. (2015) for the middle Eocene Hecho Group deposits of the deep-marine Aínsa Basin (Spanish Pyrenees), which was a tectonically active basin that formed at convergent-plate margin (Pickering and Cantalejo, 2015, and references therein). The Middle Eocene stratigraphy of the Pyrenees and adjoining areas is one of the best natural laboratories worldwide for understanding a connected sedimentary system from terrestrial, through shelf and submarine slope, to deep-marine environments in a tectonically-active basin. The Aínsa Basin occupies a critical position within the source-to-sink system, between the non-marine, marginal-marine and shallow-marine environments that acted as the sediment supply and transfer areas for sediment-transfer processes into the deep-marine environments of the Aínsa Basin, and the more distal Jaca and Pamplona basinal sinks.

There are few published chronostratigraphic studies based on the deep-marine sediments of the Aínsa Basin. Some of these studies are limited to a specific stratigraphic interval, e.g., biostratigraphy studies restricted to the Aínsa submarine-fan and related system undertaken by Pickering and Corregidor (2005), and in the Guaso System by Sutcliffe and Pickering (2009). The most complete study is that of Scotchman et al. (2015), based on calcareous nannofossil and larger benthic foraminifera age determination through ~2 km of Upper Hecho Group stratigraphy. Previous magnetostratigraphic work has been undertaken in shallow-marine sediments around the margins of the basin (e.g., Mochales et al., 2012a, b in the Boltaña Anticline, Holl and Anastasio, 1993 in the Mediano Anticline), with a synthesis and new measurements by Muñoz et al. (2013).

The deep-marine environments of the Aínsa Basin represent slope, base-of-slope and proximal basin-floor sediments (Pickering and Cantalejo, 2015, and references therein) linked to the proximal fluvio-deltaic Tresp Basin to the east and the more distal deep-marine Jaca basin to the west (Figure 1). Intra-basinal regional correlations have been attempted between the Tresp and Aínsa basins (Serra-Kiel et al., 1994; Bentham and Burbank, 1996; Nijman, 1998; Das Gupta and Pickering, 2008) and between the Aínsa and Jaca basins (Labaume et al., 1985; Payros et al., 1999; Oms et al., 2003). However, some correlations have proved to be controversial and contradictory, as discussed below. Inter-basinal correlations are also complicated by the lack of consensus on lithostratigraphic nomenclature used for the various

formation names. In addition, the Aínsa and Jaca basins are separated by the Boltaña Anticline across which Hecho Group sediments are not represented, making it considerably more difficult to establish correlations across these two basin-fills (cf. Das Gupta and Pickering, 2008; Caja et al., 2010; Clark et al., 2017).

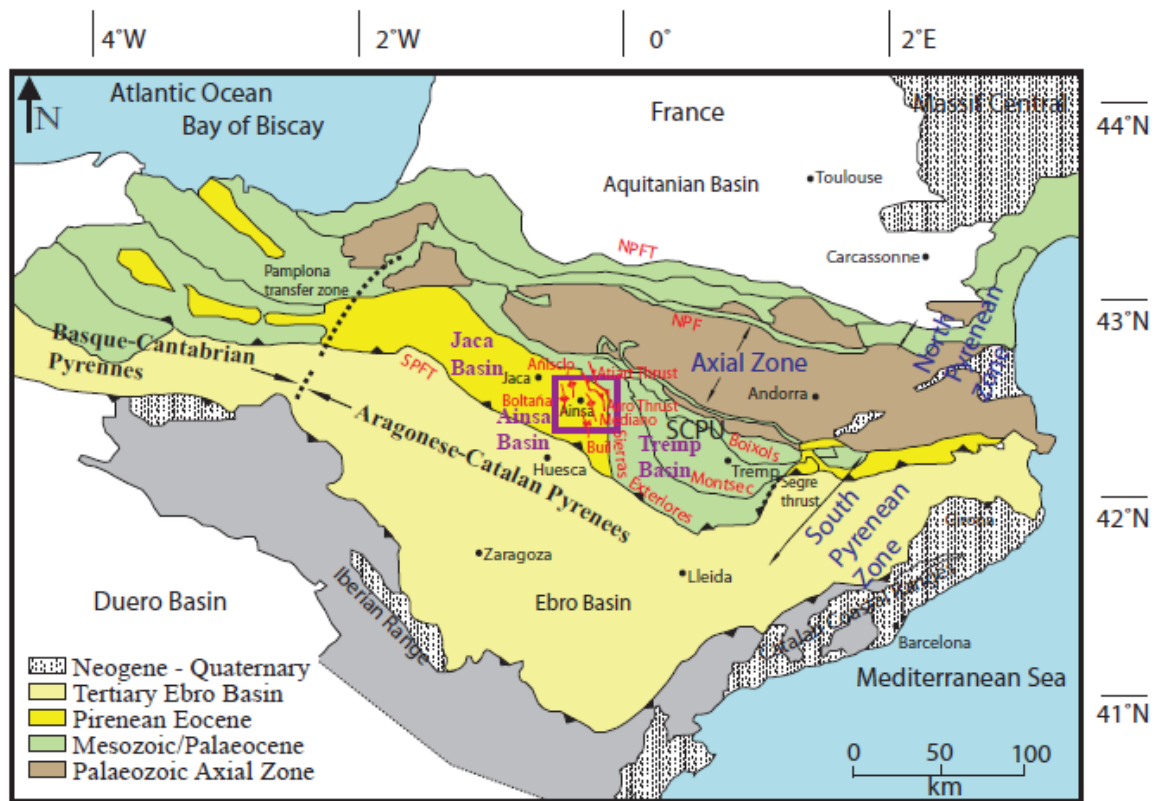


Fig. 1. Schematic geological map of the Pyrenees showing the position of the Aínsa Basin and the main tectonic structures. NPFT = North Pyrenean Frontal Thrust; NPF = North Pyrenean Fault; SPFT = South Pyrenean Frontal Thrust; SCPU = South-Central Pyrenean Unit (modified after Vergés et al. (2002)).

The main aim of this paper is to provide an integrated magneto- and biostratigraphically constrained high-resolution age model for the Aínsa Basin. This new age model: (i) presents new magnetostratigraphy in the basin to help tie the magnetostratigraphic work of Mochales et al. (2012a), Holl and Anastasio (1993) in the sediments of the Boltaña and Mediano basin flank anticlines, respectively, and also integrate the work by Muñoz et al. (2013), to the Aínsa Basin stratigraphy, (ii) provides new micropalaeontological observations across the entire

basin deep-marine stratigraphy and incorporates the previously published biostratigraphic work of Scotchman et al. (2015) in the Upper Hecho Group, and (iii) proposes new correlations with updip (Trempe) and downdip (Jaca) stratigraphy to refine the source-to-sink configurations.

The age model presented constitutes a time framework to its companion manuscript (Cantalejo et al. in review) where we investigate the role of climate change versus tectonics in modulating coarse-grained sediment flux to the basin. This manuscript discusses the temporal span of deep-marine channel and related depositional systems, and demonstrates the complex nature of drivers on deep-marine sandy fans in a tectonically-active basin.

Geological setting

The Aínsa Basin is located in the western part of the South Central Pyrenean Unit (SCPU) within the South Pyrenean Thrust System (Fernández et al., 2012). It initially developed as a foreland basin during the Ypresian-Lutetian, due to flexural subsidence caused by the advancement of the Montsec-Cotiella thrust sheet (Dreyer et al., 1999). In the middle Lutetian and Bartonian, thrust sheets propagated westwards towards the foreland and a number of north-south trending anticlines and synclines developed in the basin (Muñoz et al., 1998; Fernández et al., 2004; Muñoz et al., 2013). The Boltaña and Mediano anticlines define the western and eastern sides of the Aínsa Basin, respectively.

Palaeomagnetic studies of the Gavarnie thrust sheet by Muñoz et al. (2013) suggest regional clockwise rotations of up to 80° in sediments throughout the Lutetian with a decreasing amount of rotation. Rotation in the Aínsa Basin area was coeval with the formation of 3-km in length N–S trending anticlines (Mediano, Añisclo and Boltaña anticlines), and with the growth of extensional faults in the Montsec thrust sheet (Muñoz et al., 2013). Such growth structures during deposition of the deep-marine sediments show the importance of synsedimentary tectonics in controlling basin configuration both prior to, and during, deposition. Thus, although important synsedimentary seafloor growth structures have been identified in the area of the Mediano, Añisclo and Boltaña anticlines, and associated synclines (Puigdefábregas, 1975; Holl and Anastasio, 1993; Muñoz et al., 1994; Poblet et al., 1998; Dreyer et al., 1999; Pickering and Corregidor, 2000, 2005; Fernández et al., 2004; Mochales et al., 2012a, b; Fernández et al., 2012; Muñoz et al. 2013; Bayliss and Pickering, 2015a, b; Pickering et al., 2015), the present orientation of these tectonic features most likely

developed obliquely to the orientation of the seafloor topographic ridges that were growing during sedimentation.

The infill of the Aínsa Basin consists of ~4 km of deep-marine structurally-confined, syntectonic, delta-fed lower basin-slope and base-of-slope clastic depositional systems that accumulated during the Ypresian and the Lutetian stages of the Eocene (Figure 2) (Barnolas and Teixell, 1994; Remacha and Fernández, 2003; Fernández et al., 2004; Pickering and Corregidor, 2005; Pickering and Bayliss, 2009). These sediments constitute the Hecho Group, defined by Mutti et al. (1972) as comprising all the syntectonic Eocene sediment gravity-flow (SGF) and pelagic/hemipelagic deposits of the south-central Pyrenees that accumulated from the early Ypresian (Remacha et al., 1998) to the late Lutetian/early Bartonian (Oms et al., 2003). The deposits consist of a succession of mudstones (commonly marlstones) and coarser-grained sandbodies. The mudstones are characterised by thick intervals (up to several hundred metres thick) of thin-bedded laminated siltstones and marlstones that constitute both interfan and fan lateral-margin facies (Pickering and Corregidor, 2005; Pickering and Bayliss, 2009). Eight sand-rich, deep-marine systems have been recognised, from the oldest: Fosado, Los Molinos, Arro, Gerbe, Banastón, Aínsa, Morillo and Guaso (Pickering and Corregidor, 2005). Each of these systems contains two to six sandbodies interpreted as sand-prone channelised submarine fans and related deposits (Pickering and Corregidor, 2005; Pickering and Bayliss, 2009).

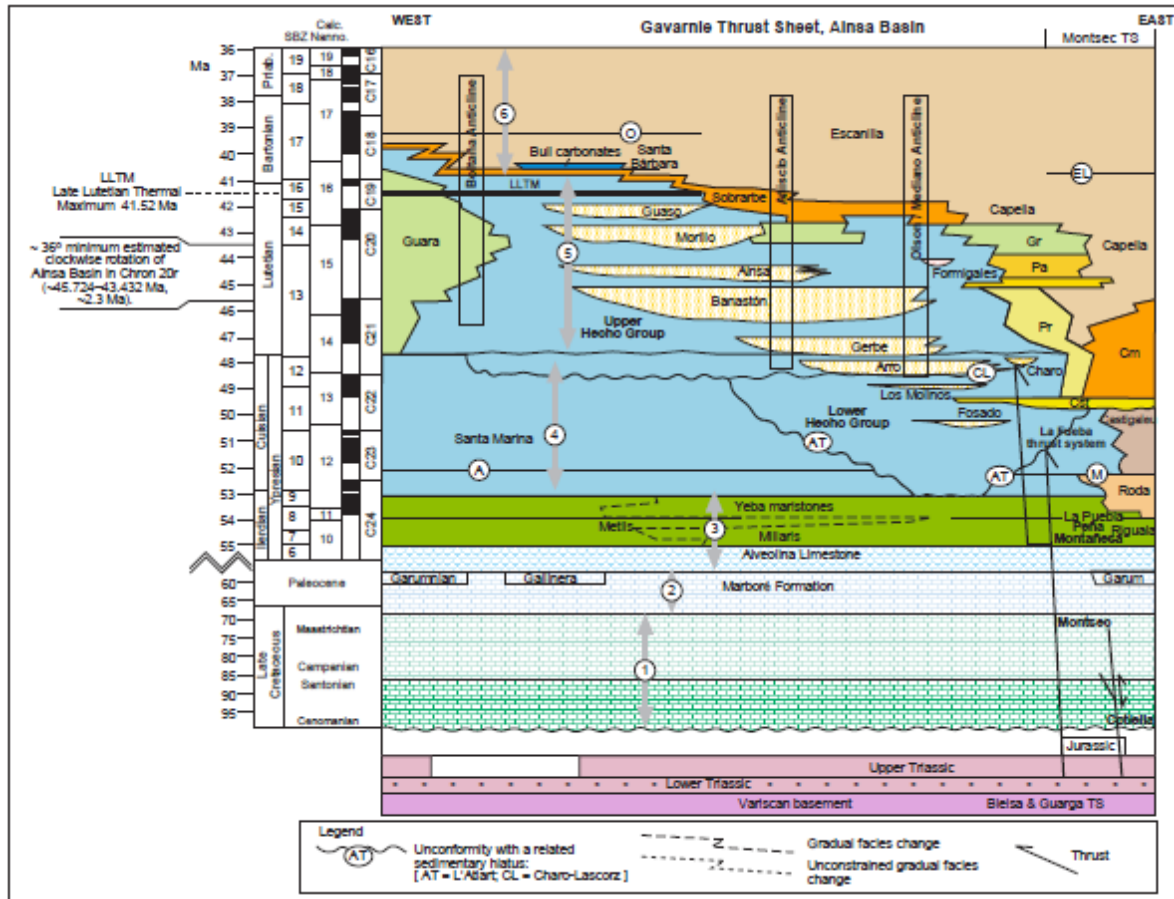


Fig. 2. Stratigraphy of the Aínsa Basin in the context of the Gavarnie thrust sheet, modified from Muñoz et al. (2013). Lithostratigraphic units: Es = Escanilla; Bu = Buil; So, Sobrarbe; Gu = Guara; Gr, Grustán; Pa = Pano; Cp = Capella; Pr = Perarrúa; Cm = Campanués; Cst = Castissent; SM = Santa Marina; Cg = Castigaleu; Ro = Roda; Yb = Yeba; Ri = Riguala; Me = Metils; Mi = Millaris; Al = Alveolina limestone. SV1- 2. Hecho Group deep-marine siliciclastic systems (= San Vicente Formation of Muñoz et al. (2013)). Horizons: O = Olsón; EL = Escanilla limestone; SB = Santa Bárbara; SP = San Pedro; SL = San Lino; M = Morillo limestone; A = Ascaso; LP = La Puebla. Thrust sheets: C = Cotiella; M = Montsec; PM = Peña Montañesa; B and G = Bielsa and Guarga; LF = La Fueba thrust system. Unconformities: AT = L'Atiart; CL = Charo-Lascorz. Litho- and chronostratigraphic information compiled from Bentham (1992), Bentham and Burbank (1996), Barnolas and Gil-Peña (2001), López-Blanco et al. (2003), Mochales et al. (2012a), Rodríguez-Pintó et al. (2012), and Serra-Kiel et al. (1994). Eocene timescale from Gradstein et al. (2012). SBZ biozones calibration to the time scale integrates data from Costa et al. (2013) and Rodríguez-Pintó et al. (2012). A prominent basin-wide m-scale black mudstone/claystone likely is the LLTM Late Lutetian Thermal Maximum dated at 41.52 Ma (cf. Westerhold et al. 2018).

Methodology

Magnetostratigraphy

Samples were collected at 10 m intervals over ~2 km of stratigraphy in order to achieve sufficient resolution to capture every polarity reversal. The average sediment accumulation rates (SARs) for the interfan fine-grained sediments in the Upper Hecho Group in the Aínsa Basin has been estimated to be between 24 and 50 cm/kyr with an average of 30cm/kyr (Cantalejo and Pickering, 2015). The sampling interval must span an interval of time >10 kyr to average out secular variation. Even for the upper SAR estimate of 50cm/kyr sampling, this sampling interval is more than sufficient to meet this criterion.

Five fine-grained continuously-exposed sections were selected throughout the basin to provide a composite section that incorporates the Gerbe, Banastón, Aínsa, Morillo and Guaso systems (Figure 3). There is some stratigraphic overlap between these sections to ensure that the entire interval was sampled, but the degree of overlap is difficult to quantify because of the lateral variability of the sandbodies and interfan successions. Supplementary material 1 shows aerial photographs for each of the sections sampled.

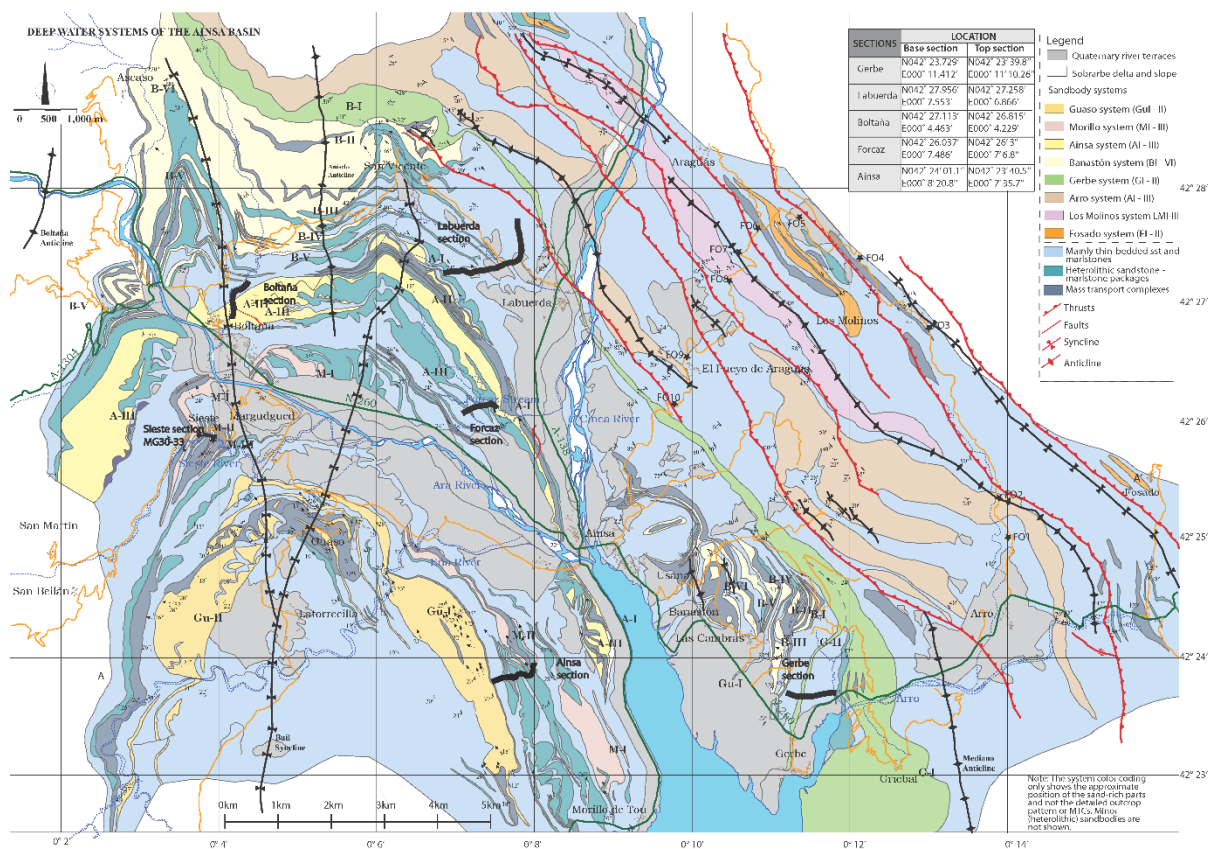


Fig. 3. Geological map of the Aínsa Basin showing the five palaeomagnetic sampling locations. In stratigraphic order, from older to younger, these sections are: Gerbe, Labuerda, Boltaña, Forcaz and Aínsa. New sampling for biostratigraphic analysis was taken every 10 m in all sections with the exception of the Aínsa section that is fully sampled in the Scotchman et al. (2015) study. The map also shows 10 additional sample sites completed in the highly deformed Lower Hecho Group (FO1-FO10) to complement previous sampling and to complete the age model of the entire Aínsa Basin stratigraphy.

Samples were collected mainly using 25 mm-diameter cores collected in the field and oriented in situ. A hand sampling technique was used at sites that were difficult to access with steep slopes that lacked a nearby water source needed to operate the drill.

Approximately two to three samples were collected per site. Hand samples were oriented using a compass clinometer. Due to size constraints, only two samples were collected per site using the hand sampling technique. The natural remnant magnetism (NRM) was measured on 415 samples of siltstones and very fine-grained sandstone turbidites (Supplementary material 2). Samples were then demagnetised using Alternating Field (AF) and/or thermal demagnetisation. Stepwise AF demagnetisation was undertaken using a 2-G Enterprises DC-SQUID (Superconducting Quantum Interference Device) cryogenic magnetometer in a magnetically-shielded laboratory at the Palaeomagnetic Laboratory at Oxford University. In order to remove any secondary NRM components, the samples were exposed in a stepwise manner with field strengths from 3 mT to progressively higher peak fields up to 100 mT. Thermal demagnetisation was used to demagnetise any magnetite or haematite present in the samples. The samples were heated rapidly at a rate of 30°C/min until a temperature of ~30°C below the desired peak temperature was achieved. Then, the samples were progressively heated at a slower rate of 10°C/min until reaching the peak temperature. This temperature was maintained for ~45 min and then the samples were cooled rapidly until they could be handled. Most of the samples were demagnetised through ~350°C. Samples were systematically rotated within the furnace to minimise laboratory acquired secondary NRM. The field orientation of the samples was corrected by inserting the strike and dip into the 2G Magnetometer software and by applying a tectonic correction factor. The data was analysed using a Super-IAPD2000. Anomalous peaks in magnetic intensities were removed from the sample paths.

PuffinPlot (Lurcock and Wilson, 2012) was used to fit lines to all data and Super-IAPD2000 (Torsvik et al., 2000) used to create stereoplots and carry out reliability tests. The quality of

the data was evaluated by using three classification categories, designated from highest to lowest quality, A, B and C (Figure 4). Category A included all samples that possess MAD (Mean Angle of Deviation) $<15\text{--}20^\circ$ and therefore showed a clear polarity and an obvious natural remnant magnetism. Category B showed a more chaotic demagnetisation trend but the general sense of polarity of the sample was still clear. It is likely that the generally low intensity magnetisation of the rock (NRM averaged values = 0.588 mA/m for the older systems (Gerbe, Banastón and Aínsa) and 0.32 mA/m in the younger systems (Morillo and Guaso) was responsible for these more chaotic trends. The weaker magnetic signals recorded by younger depositional systems may be the result of lower natural magnetic mineral delivery, perhaps due to a change of sediment source with lower magnetic mineral content. Dilution of the igneous pluton source of SGF deposit material (Das Gupta and Pickering, 2008: quartz grain provenance) could explain magnetic weakening up-section. Category C samples showed very chaotic demagnetisation trends, which prevented the visualisation of the polarity of the sample. The polarity of these samples was inferred from demagnetisation trends of other samples from the same site (repeats) or from samples immediately above or below the sampling site. 72% of the data is of sufficient quality to use in constraint of polarities (Class A and B). Data appear to be of better quality in older stratigraphic horizons. Most repeat analyses showed similar trends to the original sample, making the interpretation of the results very consistent.

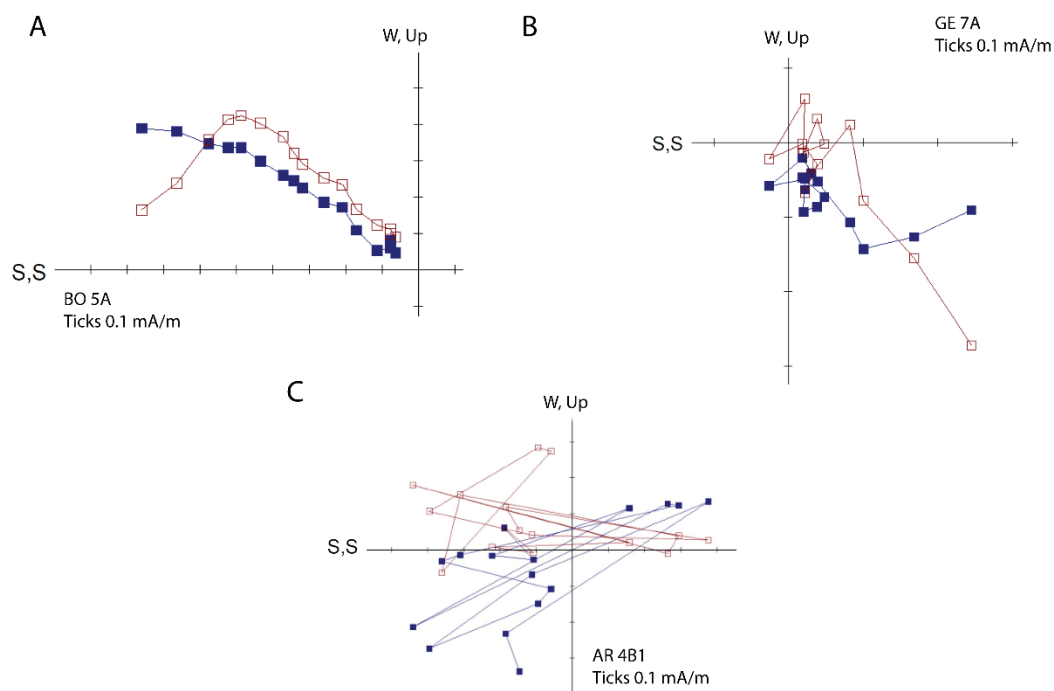


Fig. 4. Z-plots showing the three demagnetisation trend categories. The filled blue symbols show the magnitude and direction of the vectors in the horizontal plane (declination) and the open symbols show the magnitude and direction of the vector in the vertical plane (inclination). (A) Sample BO 5A of the Boltaña section showing a demagnetisation trend of category A. There is a clear demagnetisation trend indicating reverse polarity. (B) Sample GE 7A of the Gerbe section showing a demagnetisation trend of category B. Although the demagnetisation trend is more chaotic, the sample clearly shows a normal polarity. (C) Sample AR 4B1 of the Gerbe section showing a demagnetisation trend of category C. In this sample, the polarity of the sample cannot be inferred.

The declination, inclination and NRM intensity results are shown in Figure 5. The average inclination of the samples is 62.3° , giving an inferred palaeolatitude of 43.6° , similar to the present latitude of the Aínsa Basin at $\sim 42.2^\circ$. The relatively stable palaeolatitude of the area since the Eocene strengthens the reliability of the data.

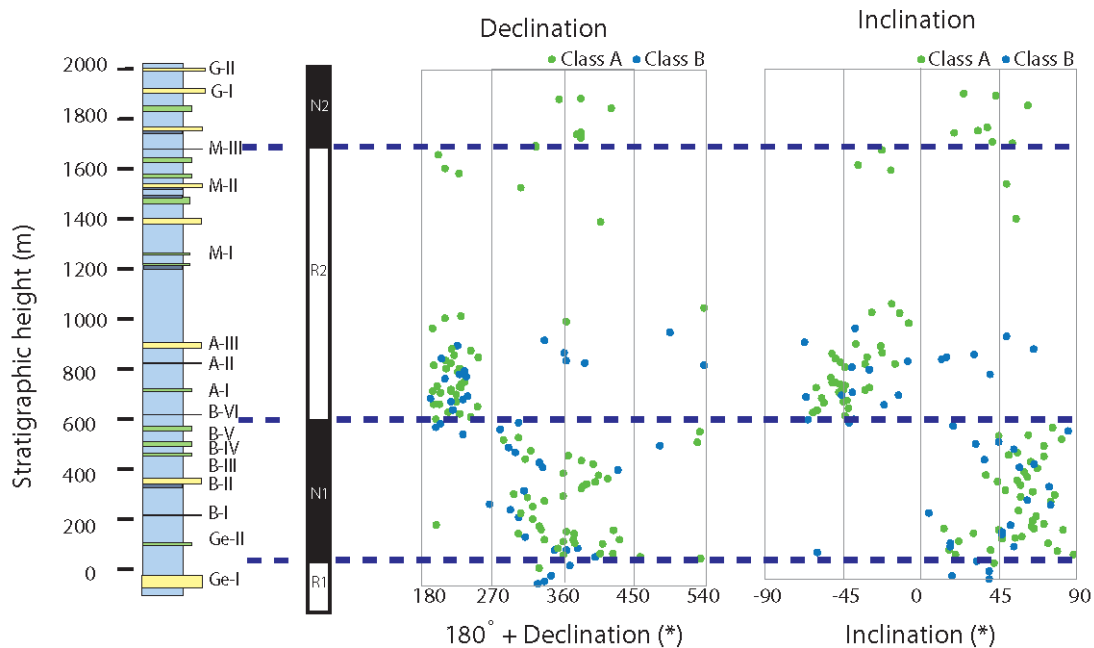


Fig. 5. Stratigraphic log of the composite Aínsa palaeomagnetic section showing polarity, inclination, declination and natural remnant magnetization (NRM) intensity. Declinations have been added to 180° to permit a clearer comparison of northward normal and southward reverse component declinations. All Class A and B sample data are fitted to stratigraphy and inferred polarity reversals. NRM averaged values are 0.588 mA/m . Grey = mudstones; yellow = sandstones, and green = heterolithics (40–60% sandstone).

In the cases where the original sample did not demagnetise to origin, most of the repeats helped to establish the polarity by showing clear demagnetisation trends. Despite this, there are thirty-one locations where none of the samples successfully demagnetised to origin. The polarity of these sites was marked with a red dot in Figure 6 indicating the uncertainty of the polarity at that specific location. Their polarity was inferred by looking at adjacent samples using stratigraphic overlaps when possible. The majority of these unresolved polarity samples were isolated and therefore could not contain a missed true reversal. This study considers a true reversal when more than one sample of different polarity is present compared with those in adjacent stratigraphy. The apparent scarcity of sampling through the upper A-III and M-I units is an artefact of the projection of data into a common stratigraphic framework that harbours large lateral variations in stratigraphic thickness between studied sections. Due to poor outcrop exposure in the Aínsa section, there are some sampling gaps in the younger part of the stratigraphy (Morillo and Guaso systems), which reduce the reliability in the upper part of the Hecho Group. In order to reduce stratigraphic gaps between the Morillo I and Morillo II interfan deposits in the Aínsa section, additional locations (MG 30-33) along the Sieste Stream (Sieste section) were sampled.

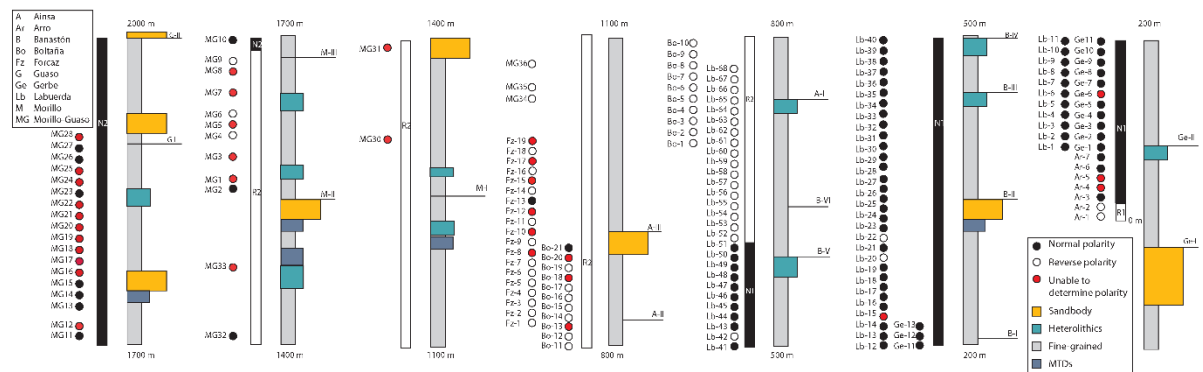


Fig. 6. Magnetostratigraphic results for the Aínsa Basin. Three polarity chrons identified as R1, N1 and R2. There are thirty-one sites where the polarity was unable to be determined (red dots). There is a clear consistency in the polarity of the overlapped sections increasing the robustness of the results.

A data table with all sample sites locations and magnetic results is included in Supplementary material 2. Note that the nomenclature for the individual samples not only refers to the collection site, but to the number of the repeats for each site and whether the samples were drilled or hand-collected.

In order to capture as complete a vertical succession as possible, a composite Aínsa Basin stratigraphy was compiled from mainly off-axis stratigraphic sections. The upper Hecho Group sediment thickness was determined from detailed measured sections (Gerbe, Banastón, Aínsa, Morillo and Guaso systems). Many of the sections show some level of overlap which ensured a continuous sampling of the stratigraphy. Where direct thickness measurements were not available they were estimated from the Aínsa Basin geological map (Pickering and Cantalejo, 2015), and converted to stratigraphic thickness using measured dips.

The clear polarity for the majority of the samples (~75%), the consistency in the polarity results of the repeat samples and in the overlapped sections, and the consistent palaeolatitude of the dataset, support the robustness and reliability of the magnetostratigraphic results from this study.

Biostratigraphy

Nannofossil samples were collected alongside those selected for palaeomagnetism analysis within the Gerbe, Labuerda, Boltaña and Forcaz sections that mainly sampled the Gerbe, Banastón and Aínsa systems. The recent biostratigraphic study of Scotchman et al. (2015), which included nannofossils and benthic foraminifera analysis in the Upper Hecho Group, was used to extrapolate the results to the Morillo and Guaso systems that were not sampled in this study. An additional ten samples (Fo1–Fo10) were collected in the Lower Hecho Group that is highly deformed and, therefore, not suitable for palaeomagnetic study, to complete the age model for the entire Hecho Group stratigraphy.

Where possible, samples were collected from unweathered outcrops of marlstones and siltstones, but fine to very fine-grained sandstones were included in areas of poor exposure. Calcareous nannofossils were analysed from sixty-one samples using simple smear slides and standard light microscope techniques (Bown and Young, 1998). Data was collected semi-quantitatively using a Zeiss Axiophot microscope at x1,000 magnification. Species abundances were estimated per field of view (FOV) after looking at least five slide transects (thousands of fields of view). Nannofossils are relatively rare in these clastic sediments and so slides were studied for a minimum of around 45 minutes. Species range charts are presented in Supplementary material 3. Taxonomy follows *Nannotax3* (<http://www.mikrotax.org/Nannotax3>). Biostratigraphy is described with reference to the Paleogene NP zones of Martini (1971) and age calibrations for individual biohorizons are

sourced from Gradstein et al. (2012)/Time Scale Creator 6.1, unless otherwise stated. The term ‘first occurrence’ (FO) is used for the first or stratigraphically lowest occurrence of the species in the section and is assumed to approximate the evolutionary appearance of the species, unless stated otherwise. The term ‘last occurrence’ (LO) is used for the last or stratigraphically highest occurrence of the species in the section and is assumed to approximate the extinction of the species, unless otherwise stated.

Results

Palaeomagnetism results

The results of this magnetostratigraphic study have identified four polarity chrons (from oldest to youngest): reverse-1 (R1), normal-1 (N1), reverse-2 (R2) and normal-2 (N2) (Figure 6).

The position of the reversal R1–N1 is based on two straddling Class B samples (from sites AR2 and AR3), carrying an overprint. Another sample was collected from the AR2 sample site (sample AR2A2A) during subsequent fieldwork shown to be consistent with this reversal. The R1–N1 reversal boundary is located ~70 m below the Gerbe II sandy fan in the interfan deposits between the Gerbe I and Gerbe II fans. The normal-1 (N1) interval is constrained between 30–610 m, from the Ar-3 site to the Lb-51 site. The stratigraphic intervals covered by this chron are the interfan successions of Gerbe I and II fans, and the Banastón I to V sandy fans. Most of the samples were of category A (45 %) and B (39 %). Six samples, all of category B, showed reverse polarity.

The N1–R2 reversal is well constrained by data with at least nine consistent-polarity samples either side of the reversal. The reverse-2 chron starts at 610 m at sample site Lb-52, in the interfan deposits between Banastón V and VI fans and continues throughout the Aínsa and Morillo fans systems until 1,677 m at sample site MG9. The R2 chron contains samples of the Labuerda, Boltaña, Forcaz, Sieste and Aínsa section and samples are ~40% Class A and 32% Class B.

The R2–N2 reversal appears to be just above the M-III fan between sample sites MG9 and MG10 (Aínsa section).

Samples at locations MG9 and MG10 (MG9A4A and MG10A2A) are both Class A (MAD values of 14.3 and 8.4, respectively), and demagnetise to the origin. MG10A2A has been substantially demagnetised with intensity reduced to ~12% of initial NRM intensity; MG9A4A less so at ~50%. Although data within this part of the stratigraphy is generally of lower quality, the reversal is clear at the scale of individual samples. Reverse polarity occurs throughout the Aínsa A-III and Morillo M-II stratigraphic intervals with five samples class A (from sites MG4, MG6 and MG9) of reverse polarity beneath the proposed R2–N2 reversal. Normal polarity is very clear above the M-III fan and in the G-I fan and interfan deposits.

Declinations and inclinations correlated with stratigraphy (Figure 5) convincingly support the N1–R2 reversal and show weak constraint of the lower R1–N1 reversal. The R2–N2 reversal is clearly apparent above 1,600 m with only two normal data points below this height opposing the proposed location of the R2 reverse chron: MG32 and MG2.

Nannofossil results

Nannofossil biostratigraphic data are presented for sixty-one new samples (Supplementary material 3). These samples complement the earlier study of Scotchman et al. (2015), which was based on sixty-seven samples incorporating stratigraphy from the Fosado to the Guaso successions. Almost all of the samples contain nannofossils that are rare to frequent, reflecting dilution of the pelagic signal by clastic sedimentary particles. Nannofossil preservation is moderate to good and the assemblages are reasonably diverse and dominated by reticulofenestrids, especially *Cyclicargolithus*. The zonal marker species are rare but in this stratigraphic interval they are large and highly conspicuous, lending confidence to our age determinations. Although reworking of microfossils frequently occurs in sedimentary basins, we are confident that the Eocene nannofossil taxa recorded here are predominantly *in situ* and indicative of depositional age because the assemblage compositions are coherent and the principal bioevents (the zonal markers) occur in the predicted order over 1000s of metres of section (see also Scotchman et al., 2015). Reworked Cretaceous nannofossils are consistently present in the samples, but are subordinate in abundance to the Eocene taxa. As Scotchman et al. (2015) have already shown, there is some offset between the nannofossil ages and those determined using larger benthic foraminifera (LBF) at the top of the section (Morillo and Guaso systems), with the latter giving slightly younger ages. This is because: (1) the LBFs are transported from shallower environments into this deep-marine basin (i.e., reworked and mixed) and this may modify the age determinations, and (2) the LBF zones are

less well-calibrated to the global magnetostratigraphic timescale. The latter factor is the most likely explanation for the discrepancies seen here.

Table 1. Summary of main biostratigraphic and magnetostratigraphic events in this *study*

Magnetostratigraphy	Stratigraphy	Sample site	System	Reversal	Age
	height				(Ma)
	2860 m	MG10	Morillo III	C20r/C20n	43.432
	1790 m	LB52	Banastón V	C21n/C20r	45.724
1200 m	AR3	Gerbe I	C21r/C21n	47.349	
Biostratigraphy	Stratigraphy	Sample site	System	Reversal	Age
	height				
	3230 m	Scotchman et al. (2015) *	Sobrarbe Delta	LO <i>S. furcat</i>	40.5
	2900 m	Scotchman et al. (2015) *	Morillo III	FO <i>R. umbilicus</i>	43.32
	2250 m	Scotchman et al. (2015) *	Aínsa III	LO <i>C. gigas</i>	44.12
	2000 m	Scotchman et al. (2015) *	Aínsa I	FO <i>S.</i> <i>furcatolithoidesplus</i>	45.33
	1900 m	BO 3	Banastón VI	FO <i>C. gigas</i>	45.49
	1500 m	LB21	Banastón I-II	LO <i>B. inflatus</i>	46.29
	1230 m	AR 4	Gerbe I	FO <i>B. inflatus</i>	47.84
	1200 m	AR 1	Gerbe I	FO <i>B. piriformis</i>	47.94
	0-1200 m	N5-N3	Fosado/Los Molinos	No <i>T. orthostylus</i>	50.5

Integrates results from Scotchman et al. (2015) *

The nannofossiliferous samples studied here from the Upper Hecho Group range from Subzone NP14b (Lutetian) in the Gerbe System (Arro Section) to Subzone NP15b (Lutetian) at the top of the Aínsa System (Forcaz Section). The key, age-diagnostic marker species are *Blackites inflatus*, *Blackites piriformis* and *Coccolithus gigas* (Table 1) but a range of additional taxa support these subzonal assignments (e.g., *Lanternithus minutus*, *Pemma spp.*, *Nannotetrina cristata*, *Sphenolithus furcatolithoides*, *S. spiniger*). Images of individual nannofossil marker taxa are shown in Figure 7. The nannofossiliferous samples from the Lower Hecho samples range from Zone NP13 (Ypresian) in the Fosado System to Subzone NP14a (Ypresian) in the Arro System. The key, age-diagnostic species are *Blackites inversus*, *Chiphragmolithus acanthodes*, *Discoaster kuepperi*, *D. lodoensis*, *D. sublodoensis*, *Lanternithus minutus* and *Pemma spp.* (Table 1).

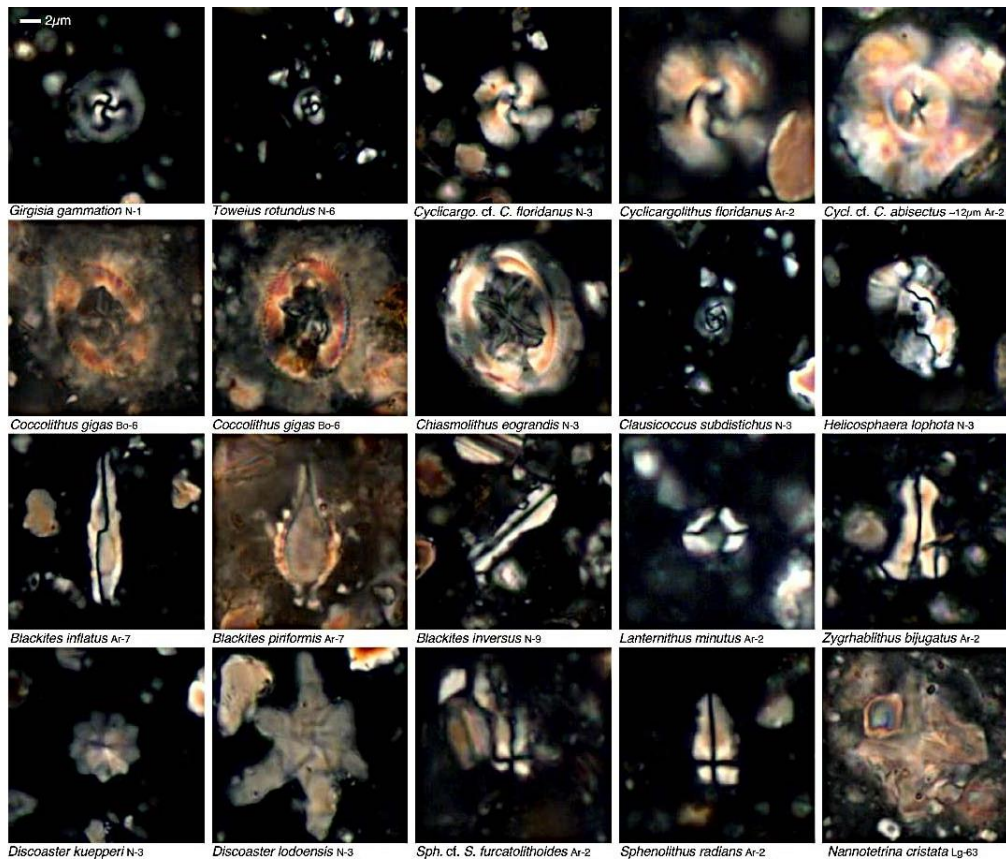


Fig. 7. Illustration of key calcareous nannofossil index species identified in the biostratigraphic samples. The letter next to the species indicate the sample location (Ar = Arro, Lg = Labuerda, Bo = Boltaña, N = lowest Hecho Group – (Fosado, Los Molinos). Scale is consistent in all samples.

Our new data are consistent with the previous work of Scotchman et al. (2015) despite the inclusion of new sections from different depositional settings within the basin. This further supports the recorded biohorizons being reliable indicators of the depositional age of the sediments.

Proposed age model

Using primarily key nannofossils markers from our biostratigraphic analysis, we have assigned the palaeomagnetic reversals identified in this study to the global palaeomagnetic time scale to construct a revised age model for the Aínsa Basin (Figure 8). This figure shows an integrated framework where we include previous biostratigraphic and palaeomagnetic work undertaken in the basin.

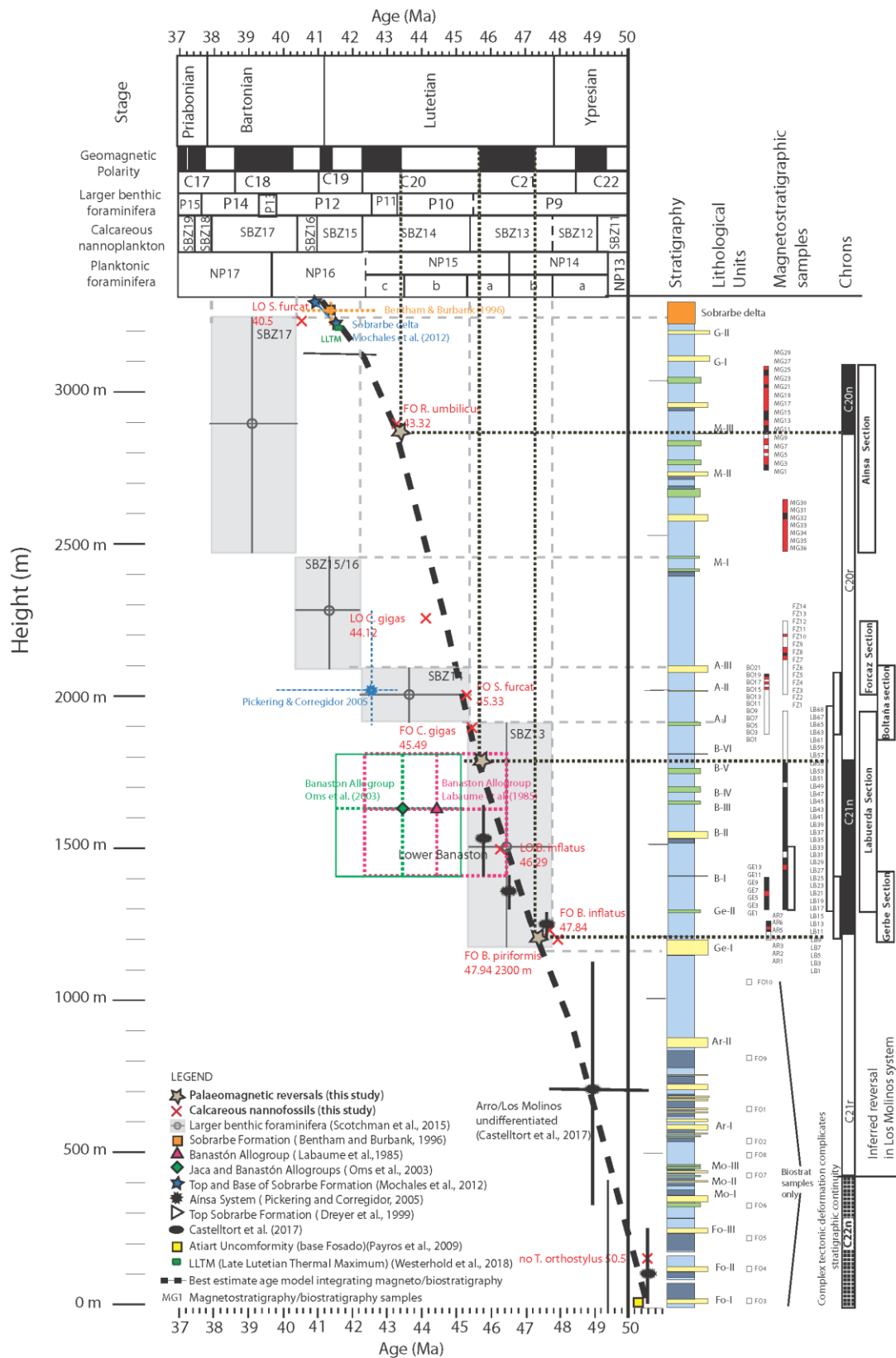


Fig. 8. Chronostratigraphy of the Aínsa Basin and comparisons with previous studies. Yellow = sandbodies; blue = mudstones/marlstones; green = heterolithics (40–60% sandstone); steel grey = MTDs/MTCs. The stratigraphic log is a composite from sections dominated by finer-

grained, muddy sediments where most of our palaeomagnetism and biostratigraphic work was undertaken. Biostratigraphy is described with reference to the Paleogene NP zones of Martini (1971) and age calibrations for individual biohorizons are sourced from Gradstein et al. (2012)/Time Scale Creator 6.1, unless stated otherwise. The term ‘first occurrence’ (FO) is used for the first or stratigraphically lowest occurrence of the species in the section and is assumed to approximate the evolutionary appearance of the species, unless stated otherwise. The term ‘last occurrence’ (LO) is used for the last or stratigraphically highest occurrence of the species in the section and is assumed to approximate the extinction of the species, unless stated otherwise.

Within this biostratigraphic framework, the best possible correlation to the palaeomagnetic scale is by associating the R1-N1 reversal identified in the interfan deposits between the Gerbe I and Gerbe II fan sandbodies to the C21r/C21n (47.349 Ma) magnetic reversal; the N1-R2 reversal identified during the deposition of the interfan deposits between Banastón V and VI sandbodies to the C21n/C20r polarity reversal (45.724 Ma) and the R2-N2 reversal just above the Morillo III Fan sandbody to the C20r–C20n reversal (43.432 Ma).

An alternative scenario, in which we shift the identified reversals to a younger part of the stratigraphy and therefore the R1-N1; N1-R2 and R2-N2 reversals become the C20r/C20n, C20n/C19r and C19r–C19n respectively, produces a significant time offset with our key nannofossils markers (Supplementary material 4). For example, FO *B. inflatus* a key marker at 47.84 Ma identified in sample AR4 within the Gerbe system produces a large time offset (~4 Myr) if we associate the R1/N1 reversal also found in the Gerbe system to the C20r/C20n reversal (43.432 Ma). In addition, the short time duration of the C19 chrons would then result in unrealistically high SARs during the deposition of the Aínsa, Morillo and Guaso systems which is inconsistent with previous publications (Cantalejo and Pickering, 2015). Similar problems are found when shifting the identified reversals to an older part of the stratigraphy, which is inconsistent within our biostratigraphy framework and with previous published work (i.e., Bentham and Burbank, 1996; Dreyer et al. 1999; Mochales et al. 2012a; Muñoz et al. 2013).

There appears to be a remarkably linear trend between age and sediment thickness (Figure 8), showing that SARs in the basin were relatively constant during the infill of the basin. The average SAR for the entire Aínsa Basin deep-marine sediments is ~39 cm/kyr, but likely to vary laterally and vertically at finer-scale resolutions across the systems due to changing

lithologies of siltstone-prone interfan sections, sand-prone sandy SGF deposits (fans) and MTDs/MTCs. The SARs variation at finer scales is analysed and discussed in Cantalejo et al., in review).

Discussion

The age of the older part of the Lower Hecho Group (Fosado and Los Molinos systems) is poorly constrained due to the severe tectonic deformation with numerous thrusts that likely duplicate and/or excise stratigraphy (Millington and Clark, 1995; Castellort et al., 2017); there are also many MTDs/MTCs. In the ten additional samples collected for biostratigraphy (FO-1 to FO10), the absence of the key nannofossil marker *T. orthostylus* suggests that the Lower Hecho Group is younger than 50.5 Ma. At the base of the Fosado system, the Atiart unconformity, an erosional surface interpreted as a submarine canyon (cf. Clark et al., 2017), is dated as 50.2 Ma (Payros et al., 2009) based on planktonic foraminifera data. This surface cuts into the shallow-marine sediments of the Castigaleu Formation and is overlain by deep-marine mudstones and thin-bedded sediment gravity-flow deposits that accumulated with the rapidly deepening Aínsa Basin. Castellort et al. (2017) consider a maximum possible age of 50.5 Ma given the presence of Zone NP13 nannoplankton in the time-equivalent Castissent Formation (Tosquella, 1995), and the identification of Chron C22r (base at 50.63 Ma) immediately below the Castissent Formation (Bentham and Burbank, 1996).

In the Arro System, detailed mapping by Millington and Clark (1995) linked the erosional surface of the Charo Canyon to the Arro deep-marine depositional system (sandy submarine fan). Biostratigraphic studies undertaken on the infill of the canyon have identified the presence of nannofossil Subzone NP15a (correlative with Chron C21n) (Payros et al., 2009). The study of Scotchman et al. (2015) suggested that the deposition of the Arro system occurred much earlier, within nannofossil Zone NP13 (correlative with Chron C22r–C22n). The C21r–C21n magnetic-reversal found within the Gerbe System succession (this study) suggests that the timing of deposition of the Arro System is more likely to have occurred within chrons C21r and C22n, supported by our new nannofossil data that places the Arro System at ~48.5 Ma (this study).

A limited palaeomagnetic study of parts of the Lower Hecho Group by Poyatos-Moré (2014) identified chrons C22 and C21 in the Lascorz/La Nata area. This study proposed that the base of the Charo-2/Lascorz unconformity (top of the Castissent sequence), defining the base of the Charo Canyon (and overlain by the Santa Siestra sequence; cf. Payros et al. 2009), is

approximately at the base of chron C21n (in agreement with the Ésera River section palaeomagnetic study by Bentham and Burbank (1996). These results are consistent with this study.

Castelltort et al. (2017) used the bulk $\delta^{13}\text{C}_{\text{carb}}$ signal, correlated with the coeval eustatic curve from the New Jersey (USA) passive margin based on the backstripped curves of Miller et al. (2005), in an attempt to provide an independent record of global sea-level changes for the Arro, Gerbe and lower Banastón systems (first presented in a pilot study for the Aínsa Basin by Das Gupta, 2008, figs 6.2, 6.4). In the Castelltort et al. (2017) study, the Arro System (Arro I and II fans) accumulated in Chron C22r, placing this system in an older part of the timescale than our estimates that place the Arro System in Chron C21r.

In the Gerbe System, a major erosional unconformity (named the Lascorz Canyon) has been linked to submarine fan deposits (Mutti et al., 1985). The Gerbe System of Mutti et al. (1985) has been correlated with the Castissent Group dated within Chron C21n, where, on the western limb of the Mediano Anticline, ~ 200 m of stratigraphy accumulated below the Lascorz unconformity within C21n (Holl and Anastasio, 1993). Using the sediment accumulation rate of 30 cm/kyr (Scotchman et al., 2015), Clark et al. (2017) estimated that this corresponds to a minimum of ~ 600 kyr, leading to their placing the Lascorz unconformity 600 m above the base of chron C21n. Payros et al. (2009) used microfossils to assign the Lascorz unconformity to shallow benthic zone SBZ13 and nannofossil subzone CP12b/NP14a. Using the time scale of Gradstein et al. (2012), Clark et al. (2017) placed the timing of the Lascorz unconformity as between 46.8–46.4 Ma. Our study shows that the Gerbe System was deposited within chrons C21r–21n with the polarity reversal at ~50–100 m above the initiation of the Gerbe System. Most of the Gerbe System therefore falls within Chron C21n.

The Banastón System occurs within chron C21n with the C21n–C20r polarity reversal identified between the Banastón V and VI interfan deposits. The deep-marine Banastón System has been linked to the Formigales Canyon located at the eastern edge of the Aínsa Basin (Mutti et al., 1985). This canyon erodes underlying deltaic sediments of the Capella Formation that has been dated within chrons C21n and C20r (Cuevas-Gonzalo, 1989; Bentham and Burbank, 1996). The results from this study support the interpretation that the

Formigales Canyon was probably active during the deposition of the Aínsa and Morillo systems.

Our age dating for the Aínsa System differs with that of Remacha et al. (2003) who proposed a younger depositional age within foraminifera zones P12–P13 (~nannofossil zone NP16). Recent biostratigraphic studies by Scotchman et al. (2015) suggest that deposition of the Aínsa System occurred within nannofossil zone NP15 (broadly in agreement with Pickering and Corregidor, 2005) and shallow benthic zone SBZ13, correlative with Chron C20r. Our magnetostratigraphic work shows reverse polarity throughout the Aínsa system. Scotchman et al. (2015) inferred the C21n–C20r magnetic reversal to be at the base of the Aínsa System; however, we show that the reversal occurred slightly lower in the stratigraphy within the Banastón V and VI interfan deposits, suggesting that the sediments of the Aínsa System are younger by ~1 Myr than that of Remacha et al. (2003). Our revised age estimates place the deposition of the Aínsa System at ~45–44 Ma, between the estimations of Pickering and Corregidor (2005) and Remacha et al. (2003). Thus, the persistent reverse polarity of the Aínsa system together with the position of the first occurrences of the nannofossils *S. furcatolithoide* and *C. gigas* first identified by Scotchman et al. (2015), supported by our new biostratigraphic analysis here, place the Aínsa System within Chron C20r.

The Morillo System is characterised by reverse polarity (C20r) with the C20r–C20n polarity reversal at 43.432 Ma, located just above the Morillo III Fan sandbody. Scotchman et al. (2015) dated the Morillo System as within nannofossil zone NP15–NP16 and shallow benthic foraminifera zone SBZ14–SBZ15 or 43.2–44.24 Ma. Mochales et al. (2012a) estimated the end of the Morillo System at 43.2 Ma.

The top of the Guaso System represents the termination of the deep-marine deposition and the beginning of the deposition of deltaics and fluvial deposits of the Sobrarbe and Escanilla formations within the Aínsa Basin. The initiation of the Guaso System appears to have been at ~43.23 Ma (Pickering and Corregidor, 2005; Scotchman et al., 2015). The cessation of the deep-marine sedimentation has been estimated to be between 41.6–42.3 Ma in SBZ15 and at the top of Chron C20n (Bentham and Burbank, 1996; Dreyer et al., 1999; Mochales et al., 2012a). Scotchman et al. (2015) suggested the top of the Guaso System to be a dark-shale anoxic horizon estimated at 42.55 Ma. In our proposed age model for the Aínsa Basin this prominent basin-wide m-scale black mudstone/claystone, unique to the basin, and that we have mapped above the youngest sandbody in the Guaso System, and immediately below the

Sobrarbe deltaic system, is dated at ~41.5 Ma. This same band was called the "Anoxic Level" by Mochales et al. (2012a) and dated at ~41.6 Ma (also noted in Scotchman et al., 2015). This ~3-m thick dark mudstone unit is likely to be the ~30-kyr Late Lutetian Thermal Maximum (LLTM) that is recognised as a global transient warming event, dated from Atlantic deep-sea cores at 41.52 Ma by Westerhold et al. (2018). Time-series analysis of the mudrocks in the Aínsa Basin indicate sediment accumulation rates of ~30 cm/kyr (Cantalejo and Pickering, 2015), consistent with the thickness of the dark mudstone/claystone as the LLTM.

The age of termination of the deep-marine sedimentation of the Hecho Group with Remacha et al. (2003) is ~41 Ma in the Jaca Basin and Scotchman et al. (2015) estimated it at ~42 Ma in the Ainsa Basin. Here we have shown that the sediments of the Gerbe, Banastón and Ainsa system sediments are ~1 Myr younger than the age model proposed by Scotchman et al. (2015). If this relationship is maintained throughout the younger systems, then the termination of the Hecho Group deposition would be coeval in both basins at ~41 Ma.

Synsedimentary basin rotation

We interpret smearing of normal polarity data to result from a change in declination during chrons C21n, C20r and C20n (Figure 9), offsetting Chron C20n to the west relative to the earlier C21n. This shows that the basin was rotating during deposition of the Hecho Group sediments (Figure 10).

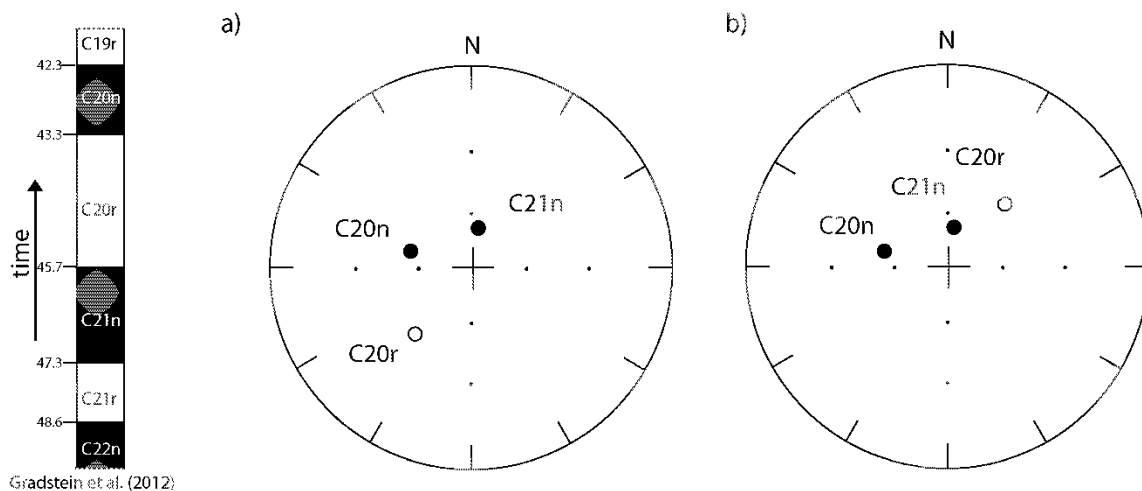


Fig. 9. (a). Magnetic Directions ChronMeans. Stereonets to show tilt-corrected amalgamated Class A data chron mean directions (Super-IAPD2000: Torsvik et al. 2000). (a) shows true mean directions whereas in (b) Chron C20r has been inverted so all directions are of normal

polarity, allowing comparison. The GPTS according to Gradstein et al. (2012) is included to allow reference of relative chron positions.

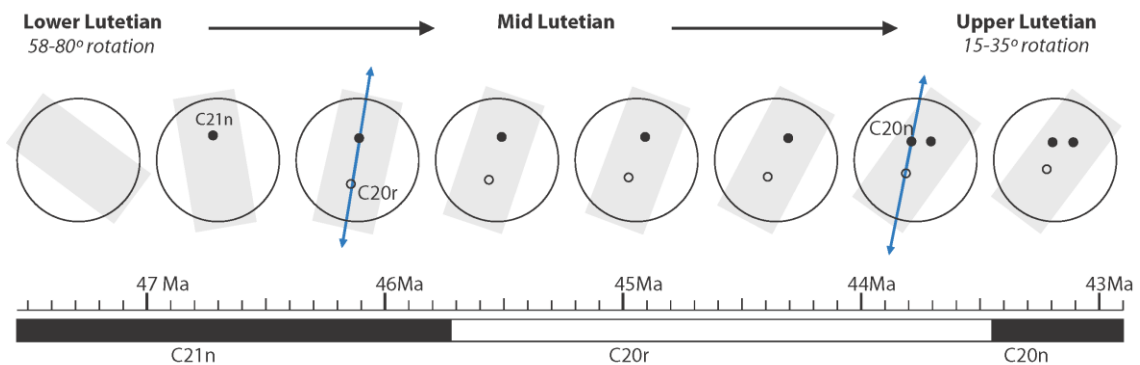


Fig. 10. Cartoon to schematically conceptualize synsedimentary basinal rotation: grey rectangles show general sampling region rotation; circles represent N-up stereonets and black/white dots, acquired normal/reverse polarity means respectively; blue arrows show polarity reversal axis. Chron C21n-age sediments are deposited during fast rotation rates, the Earth's magnetic field reverses and Chron C20r-age sediments form during slower rotation of the basin, the field reverses back to normal polarity but due to rotation Chron C20n-aged sediments possess declinations more westerly than those of Chron C21n. This results in smearing of normal polarity directions.

From palaeomagnetic analyses, Muñoz et al. (2013) deduced synsedimentary clockwise rotation of the Aínsa Basin of decreasing magnitude throughout the Lutetian: rotations on the Mediano Anticline decreased from 58–80° to 15–35° (lower to upper Lutetian). Our minimum estimation for rotation during Chron C20r (45.724–43.432 Ma, 2.3 Ma duration) is 36° clockwise (Figure 11).

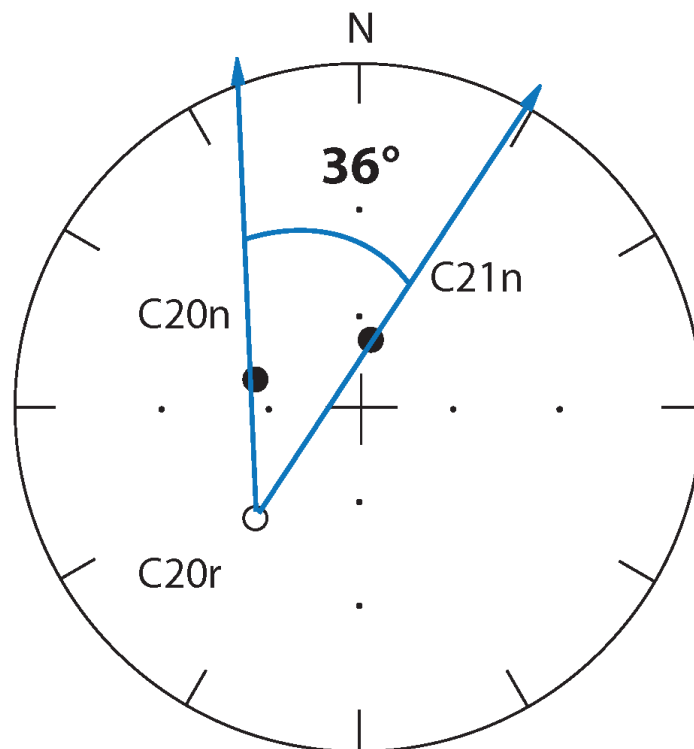


Fig. 11. Quantification of minimum rotation during Chron C20r from stereonet of chron means and the model we propose.

Palaeomagnetic studies from the Boltaña Anticline suggest a clockwise rotation of $\sim 52^\circ$ during Ypresian to Priabonian time (Mochales, 2010, 2012b). Rotation velocities fit a logarithmic model and show a low rate during the Ypresian–middle Lutetian interval ($\sim 1^\circ/\text{Myr}$) and much higher rates (up to $10^\circ/\text{Myr}$) in the late Lutetian–Priabonian interval. Thus, the most rapid and largest rotations appear to have occurred during deposition of the youngest deep-marine sediments of the basin and into the deltaic deposition of the Sobrarbe Formation (~ 42 Ma) and fluvial deposition of the Escanilla Formation (~ 35 Ma). The rotation was likely linked to movement along the base of the Gavarnie thrust sheet detached at lower Triassic Keuper evaporites below the Tethyan carbonates (Farrell et al., 1987; Muñoz, 1992; Teixell, 1996).

Such large rotations of the Gavarnie thrust sheet from early Lutetian to late Bartonian suggest that the Aínsa Basin was already a thrust-top basin and that subsidence cycles were driven by more complex tectonic mechanisms than simple repeated phases of flexural loading (e.g., “seesaw tectonics” of Pickering and Bayliss, 2009), at least for the Upper Hecho Group.

Stratigraphic correlations with the flanks of the Aínsa Basin

The age model presented in this study allows us to correlate the deep-marine stratigraphy of the basin with the stratigraphy at the flanks of the basin where Mochales et al. (2012a) and Holl and Anastasio (1993) completed a palaeomagnetic study in the western and eastern flanks, respectively.

The magnetostratigraphic study by Mochales et al. (2012a) sampled ~2.4 km of Cenozoic sediments cropping out around the Boltaña Anticline. The lateral equivalents of the deep-marine deposits of the Hecho Group are the shallow-marine deposits of the Boltaña (Barnolas et al., 1991) and the San Vicente formations (Van Lunsen, 1970). These formations are well represented in the Coscollar section, located on the eastern limb of the Boltaña Anticline. Figure 12 compares the magnetostratigraphic results of Mochales et al. (2012a) and this study. The lower part of the Upper Hecho Group (Gerbe, Banastón and Aínsa systems) appear to correlate with the Paules Member of the San Vicente Formation, while the Morillo and Guaso systems are likely to correlate with La Patra Member.

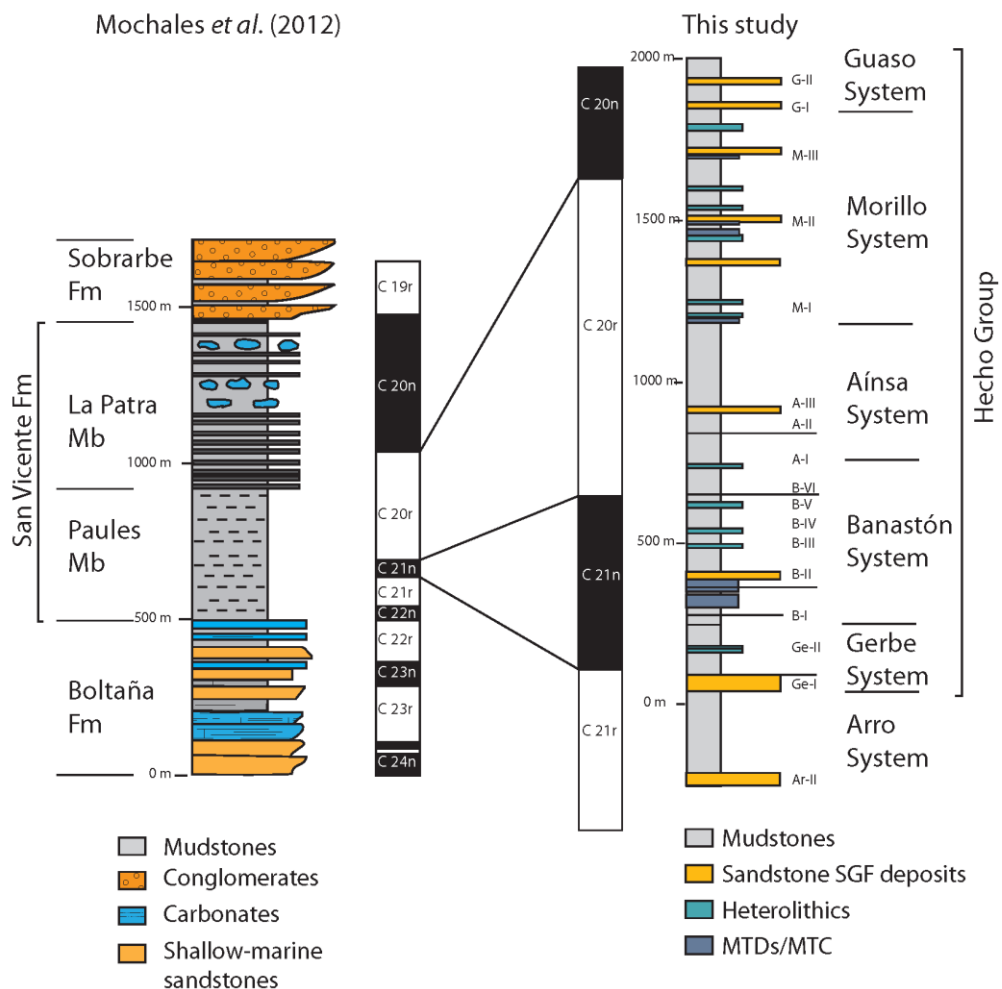


Fig. 12. Magnetostratigraphic correlation between Mochales et al. (2012a) and this study. Simplified stratigraphy of the Boltaña Anticline from Mochales et al. (2012).

SARs at the flank of the basin estimated by Mochales et al. (2012a) are in the order of 2–5 cm/kyr, whilst the SARs in the Aínsa Basin for the same interval are estimated to be ~39 cm/kyr (this study). The order of magnitude difference in SARs between the flanks of the basin and the main basin depocentre suggests that the flanks were actively growing during the deposition of the deep-marine Hecho Group.

The upper part of the Paules Member shows a significant increase in SARs from 2–5 cm/kyr to ~18 cm/kyr (Mochales et al., 2012a). Facies interpretation suggests that the Upper Paules Member is a progradational sequence (De Federico, 1981; Mochales et al., 2012a), reflecting a fall in relative sea level. In the Aínsa Basin, this interval correlates with the deposition of the Aínsa and Morillo systems which show increased structural confinement in relation to previous deep-marine systems (Pickering and Corregidor, 2005; Bayliss and Pickering, 2015a, 2015b). During this time, the basin was incorporated into the hangingwall of the Gavarnie-Sierras Exteriores Thrust (Muñoz et al., 1998; Dreyer et al., 1999; Fernández et al., 2004; Fernández et al., 2012) and as a result, the Boltaña and Mediano anticlines underwent a period of growth (Fernandez et al., 2012), which probably resulted in a progradational sequence in the Boltaña area and an increase in confinement of the deep-marine basin (Bayliss and Pickering, 2015a, 2015b). The palaeomagnetic study of Holl and Anastasio (1993) was undertaken on syn-orogenic strata in the areas surrounding the Mediano Anticline, located on the eastern edge of the Aínsa Basin. Sediment gravity flow deposits (mainly turbidites) and mudstones are exposed at the flanks of the anticline and show angular unconformities caused by times when structural growth outpaced sedimentation rate. The stratigraphic formations sampled in the study include the Castissent Group, the Santa Liestra Group and the lower part of the Campodarbe Group (after Mutti et al., 1988). Although, the study presents data from both limbs of the Mediano Anticline, only the western limb is shown in Figure 13.

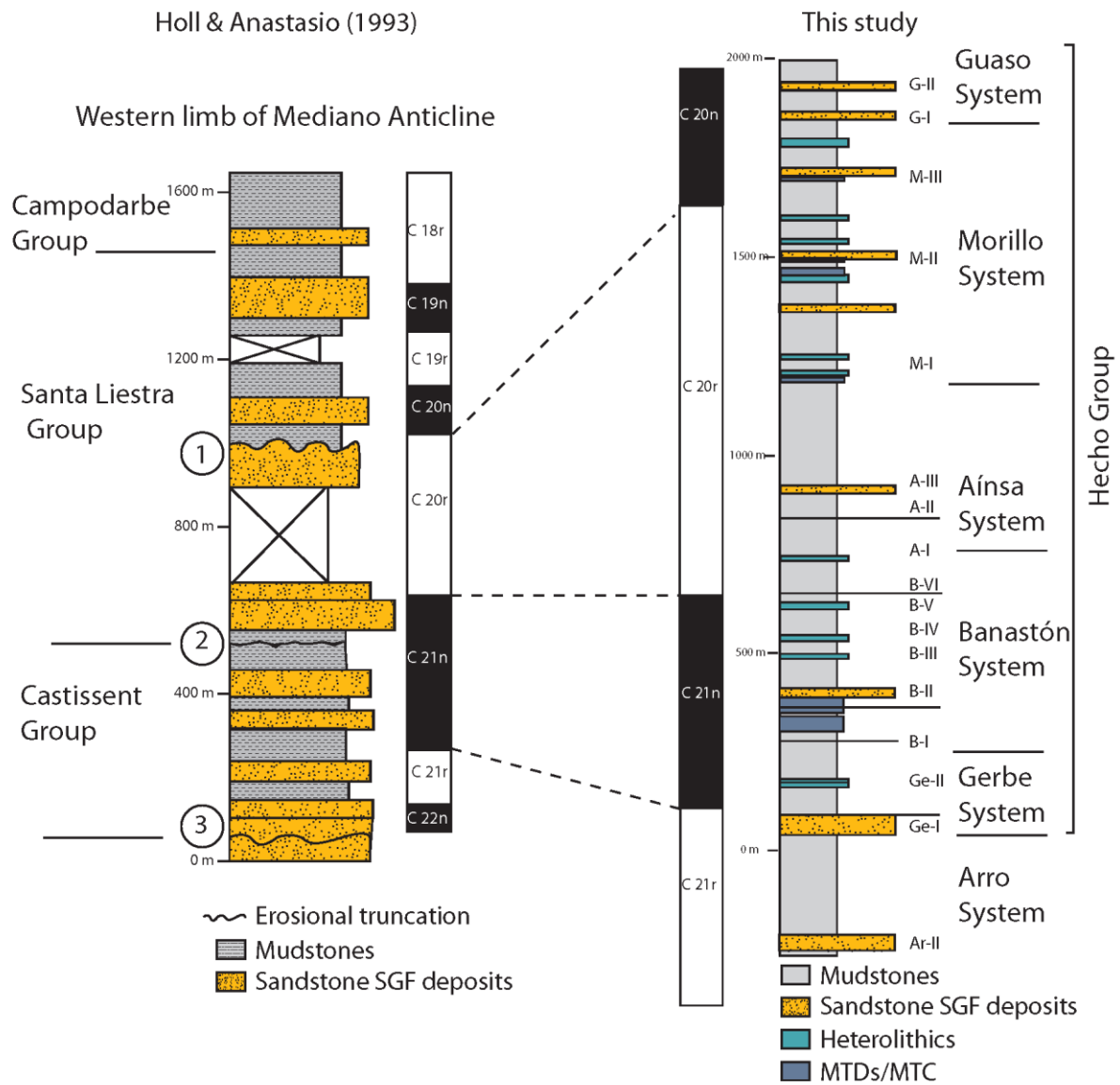


Fig. 13. Magnetostratigraphic correlation between Holl and Anastasio (1993) and this study. The Castissent Group have the same age as the Gerbe and Banastón deep-marine systems. The upper part of the Upper Hecho Group (Aínsa, Morillo and Guaso systems) can be correlated with the Santa Liestra Group.

Correlations between the study of Holl and Anastasio (1993) and this study suggest that the Gerbe and part of the Banastón System (probably BI–BIII) are coeval with the Castissent Group cropping out at the Mediano Anticline (Figure 13). The Santa Liestra Group includes the sediments equivalent to the Aínsa, Morillo and Guaso systems.

Correlations between the Jaca and the Aínsa basins

Correlations between the Aínsa and the more distal Jaca basins have proven to be difficult with palaeomagnetic and biostratigraphic studies showing conflicting results. The palaeomagnetic study undertaken by Oms et al. (2003) sampled the deep-marine clastics of the Hecho Group in the Jaca Basin. The study covered a ~2.2 km thick composite section and used previous biostratigraphic work by Labaume et al. (1985), Canudo and Molina (1988), and Payros et al. (1999), to constrain their magnetostratigraphic results, although some of these studies have shown inconsistent correlations. The lower part of the section sampled the Santa Liestra Allogroup (Cotefablo SGF deposits). These sediments are overlain by the Banastón Allogroup which includes deep-marine clastic depositional systems and carbonate megabreccias (originally referred to as "megaturbidites", but that we would now call "concentrated density-flow deposits" and "cohesive-flow deposits" in the classification scheme of Pickering and Hiscott, 2016). The upper part of the section is characterised by channelised SGF deposits (Rapitán System of Remacha et al., 1995), followed by prodelta deposits (Larres marls Formation) and platform deposits (Sabiñánigo sandstone Formation) (Puigdefábregas, 1975) (Figure 14).

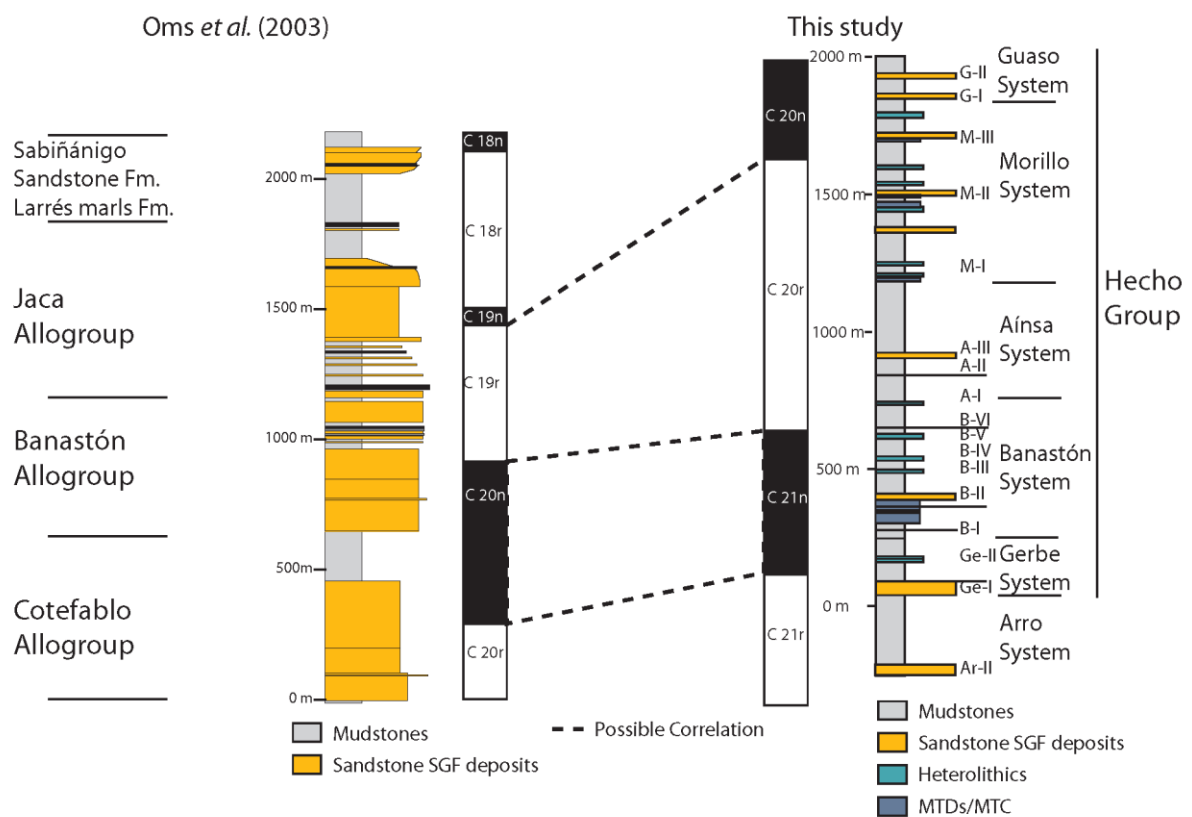


Fig. 14. Magnetostratigraphic correlation between Oms et al. (2003) and this study. Sedimentary logs reproduced after Remacha et al. (2003). Slashed lines show a possible correlation between the interpreted magnetostratigraphic data of Oms et al. (2003) and this study. The R1 interval of Oms et al. (2003) originally assigned to Chron C20n is now reinterpreted to C21n.

Oms et al. (2003) suggested that the reversed polarity observed in the lower "Cotefablo Allogroup", in agreement with biostratigraphy, can be associated with Chron C20r. This would suggest a correlation with the uppermost part of the Banastón System (Banastón VI Fan sandbody) and the Aínsa System (Figure 15). This correlation is not consistent with interbasinal correlations based on biostratigraphic and petrographic studies.

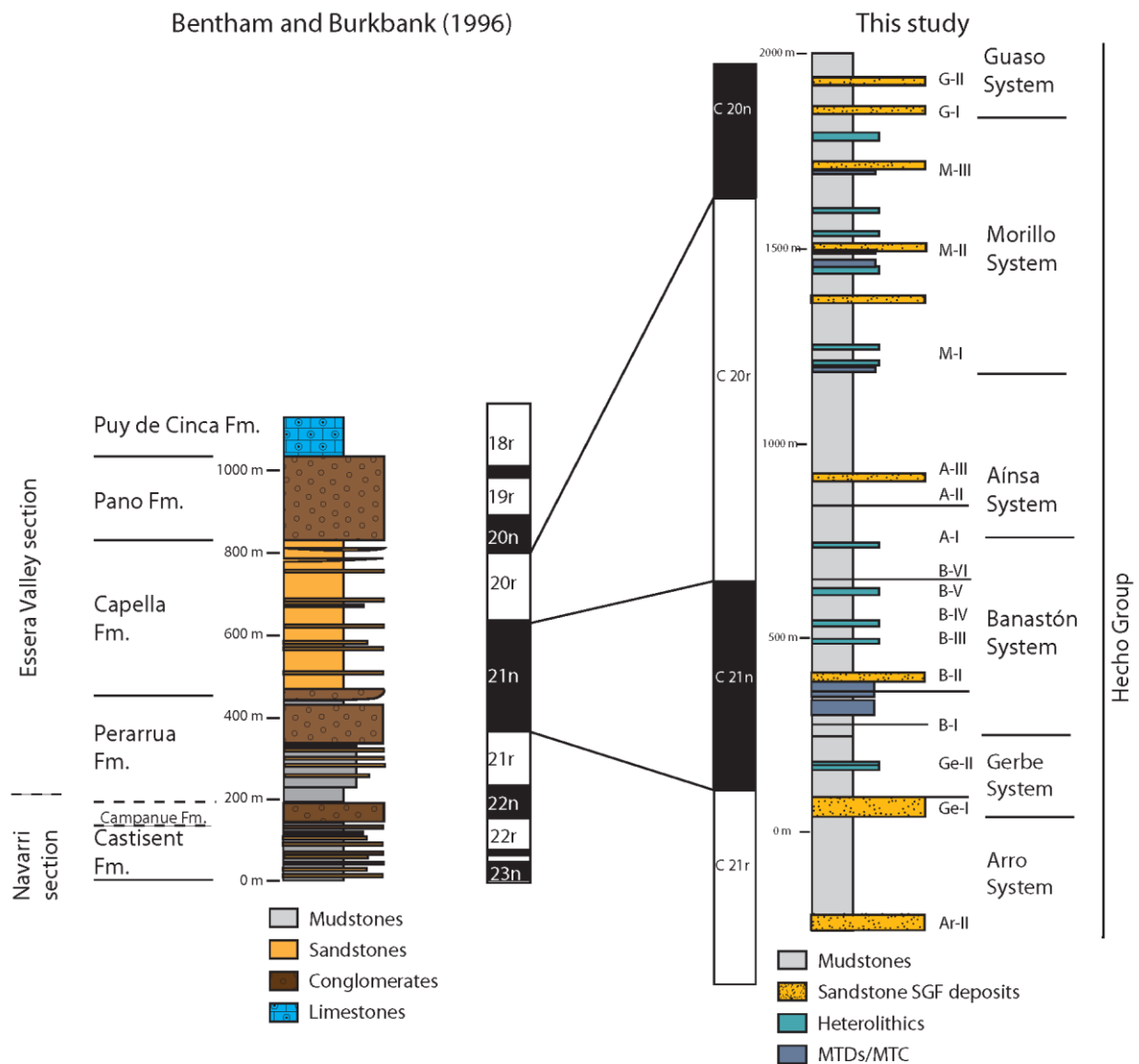


Fig. 15. Magnetostratigraphic correlation between Bentham and Burbank (1996) and this study. The Gerbe System is coeval with the Perarrua Formation and the Banastón and the Aínsa systems are coeval with the sediments of the Capella Formation. The Morillo and Guaso systems are likely to be coeval with the conglomeratic units of the Pano Formation.

The “Banastón Allogroup” has been correlated with the Banastón System using petrographic comparisons (Das Gupta and Pickering, 2008; Caja et al., 2010). Also, Payros et al. (1999) and Labaume et al. (1985) identified planktonic foraminiferal Zone P9 in the Megaturbidite 4 (MT-4), implying that MT-5 occurred within Chron C20r. If correct, this would suggest that the Cotefablo Allogroup is associated with Chron C21r instead of Chron C20r (a possibility also considered by Oms et al., 2003). Remacha et al. (2003) place the initiation of the Banastón Allogroup close to the polarity reversal between C21r–C21n with most of the Banastón Allogroup placed within Chron C21n.

Clark et al. (2017) proposed correlations between the Aínsa and Jaca basins based on bed correlations and field mapping. They proposed that the MT-4 carbonate "megaturbidite" in the Jaca Basin can be traced into the youngest part of the Morillo System in the Aínsa Basin. This led the authors to correlate the Cotefablo System above the MT-4 to the base of the Guaso System. This correlation is clearly irreconcilable with our age model that correlates the Cotefablo System in the Jaca Basin with the Morillo System in the Aínsa Basin.

Field mapping correlations are problematic across the Boltaña Anticline, which was an actively growing and rotating during deep-marine sediment accumulation in the Aínsa and Jaca basins (Pickering and Corregidor, 2005; Mochales et al. 2012a,b). This is particularly true for the Upper Hecho Group, including during the deposition of the Morillo and Guaso systems. Syn-depositional growth of the Boltaña Anticline has led to many beds showing pinch-out relationships onto the Boltaña topographic high consisting of older carbonates, and mixed carbonates and siliciclastics, thereby increasing the uncertainty in any physical correlation across the anticline for these younger systems (i.e., the Upper Hecho Group). The Lower Hecho Group is not present in the western part of the Aínsa Basin, meaning that in the order of 3-4 million years of stratigraphy is absent due to non-deposition or as very condensed sections on the flanks of the Boltaña Anticline, and/or gravitational sliding and slumping (Pickering and Corregidor, 2005; Mochales et al., 2012a). Relatively narrow sediment pathways created connections between both the Aínsa and Jaca basins, but exposure is limited and too discontinuous to allow for accurate mapping and correlation. Post-

depositional uplift of the Boltaña Anticline has removed beds that might have been deposited in this telecommunication. Establishing reliable correlations using MTDs as key horizons is complicated by the fact that it is likely that multiple local failure events occurred along the flanks of the Boltaña Anticline during its growth and rotation. Many MTDs occur around the village of Castellazo, and in the Rio Sieste (Morillo System), cited by Clark et al. (2017) as key locations for correlating MT-4 (MTD or MTDs) from the Jaca to Aínsa basins (see Supplementary material 5). We suspect that these MTDs, although below the Guaso System and apparently coeval with the carbonate MTD/MTC in the upper Morillo System, may have been deposited during separate slope-failure events that have amalgamated or created shingled depositional events that superficially appear as a single and continuous event.

Figure 14 shows our stratigraphic correlations between the Aínsa and Jaca basins, using the palaeomagnetic study from the Jaca Basin-fill of Oms et al. (2003) and the magneto- and biostratigraphy in this study.

Correlations between the Tremp and Aínsa basins

The two most important chronostratigraphic studies undertaken in the Tremp Basin are the study by Nijman (1998) based on sequence stratigraphic correlations and the study by Bentham and Burbank (1996) which included extensive magnetostratigraphic work.

The deep-marine sediments of the Aínsa Basin were sourced from a large fluviodeltaic complex which entered the Tremp-Ager Basin from the east forming the Montañana Group (Mutti et al., 1985; Marzo et al., 1988). Nijman (1998) divided the Montañana Group into the Lower Montañana (LM), Middle Montañana (MM) and Upper Montañana (UM) groups. The Lower Montañana Group (Castigaleu Formation) can be subdivided into two megasequences (LLM and ULM) and this group is characterised by trunk river sheet sandstone facies (Nijman, 1998). The Middle Montañana (Castissent Formation) only contains one megasequence. This group is characterised by amalgamated sheet sandstones typical of the main channel fluvial feeders. The Upper Montañana Group is subdivided into five megasequences (UMA-UME) and contains the Capella and the Perarrua formations.

Three main fan-delta systems were active during the accumulation of the Hecho Group SGF deposits, namely the Claramunt, San Esteban and Campanúe fans (Nijman, 1998). These fans are composed of coarse-grained sandstones and conglomerates (Puigdefábregas et al., 1992;

Nijman, 1998). The San Esteban Fan was active during the initiation of the Montaña Group and prograded significantly into the Middle Montaña Castissent fluvial environment. This fan continued its activity during the lower part of the Upper Montaña. The Campanué Fan dominated the base of the UMB megasequence.

The study undertaken by Bentham and Burbank (1996) used magnetostratigraphy in four related sections that encompass ~8 km of strata with a total of 300 magnetic sampling sites in the Tresp-Ager and the Aínsa basins. These authors only differentiated the deep-marine sediments of the Hecho Group from the overlying deltaics of the Sobrarbe Formation, and did not attempt to break down the Hecho Group into the different deep-marine systems. As a consequence, the correlations established between these two basins are broad scale and cannot resolve the age uncertainties of the individual systems (Figure 15). Their data suggest that the Gerbe System correlates with the Perarua Formation in the Upper Montaña Group, and that the older systems Los Molinos, Fosado and Arro correspond with the Middle Montaña Castissent Formation and probably the upper part of the Lower Montaña Group. The Banastón and the Aínsa systems appear coeval with the sediments of the Capella Formation in the Upper Montaña Group, and the Morillo and Guaso systems are likely to correlate with the conglomeratic units of the Pano Formation (Figure 15).

Figure 16 shows a summary of all the multiple biostratigraphic and/or magnetostratigraphic age model studies conducted in the Tresp, Aínsa and Jaca basins. Many of these studies have been discussed in detail in this manuscript. The figure also highlights the lack of consensus in the nomenclature of the different formations which poses a problem when trying to establish correlations between the different studies.

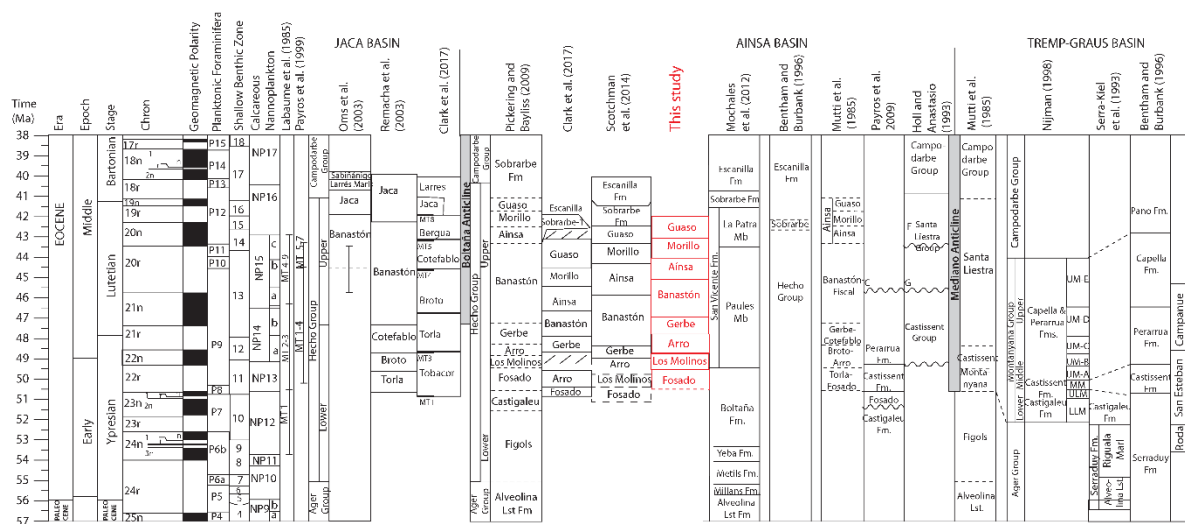


Fig. 16. Summary of chronostratigraphic work undertaken in the Jaca, Aínsa and Tremp basins showing inter-basin correlations. Results from this study are highlighted in yellow. Modified after Scotchman et al. (2015).

Conclusions

This paper presents the first magnetostratigraphic study of the deep-marine sediments of the Upper Hecho Group in the Aínsa Basin, including most of the Gerbe System and the Banastón, Aínsa, Morillo, and part of the lower Guaso, systems. We identified four main polarity chrons: R1, N1, R2 and N2 that we have interpreted as chrons C21r, C21n, C20r and C20n, using primarily nannofossil biostratigraphy. These correlations suggest that the sediments are ~1 Myr younger than the age model of Scotchman et al. (2015). The SARs during the deposition of the Upper Hecho Group average ~39 cm/kyr. Results from this study have been compared with the magnetostratigraphic studies carried out by Mochales et al. (2012a, b), and Holl and Anastasio (1993) along the margins of the Aínsa Basin, in the Boltaña and in the Mediano anticlines, respectively. In the Boltaña Anticline, the shallow-marine retrogressive sequence of the lower part of the Paules Member has been linked with the deposition of the Gerbe and the Banastón systems whilst the progradational sequence of the upper part of the Paules Member is correlated with the deposition of the Aínsa and Morillo systems. Comparisons with the study of Holl and Anastasio (1993) in the Mediano Anticline suggest the Gerbe and part of the Banastón systems (probably BI–BIII fans) are coeval with the Castissent Group and that the Aínsa, Morillo and Guaso systems are of a similar age as the Santa Liestra Group. A re-assignment of the chrons, as suggested in Clark et al. (2017), would be inconsistent with the published palaeomagnetic work of Bentham and Burbank (1996), Dreyer et al. (1999), Remacha et al. (2003), Mochales et al. (2012a), and of Muñoz et al. (2013, fig. 4). It would also make the Sobrarbe deltaic system Bartonian in age rather than Lutetian.

Our palaeomagnetic study shows a minimum 36° clockwise rotation of the Aínsa Basin during Chron C20r (~45.724–43.432 Ma, ~2.3 Ma duration), i.e., during deposition of the Hecho Group. Palaeomagnetic studies of the Gavarnie thrust sheet in the Aínsa Basin area suggest regional clockwise rotations of up to 80° in sediments of Lower Eocene age (Muñoz et al., 2013); the amount of rotation decreases with age. Rotation in the Aínsa Basin area was coeval with the growth and tightening of the Mediano, Añisclo and Boltaña anticlines, and

with the growth of extensional faults in the Montsec thrust sheet (*ibid.*). Such growth structures during deposition of the deep-marine sediments show the importance of synsedimentary tectonics in controlling basin configuration both prior to, and during, deposition.

We thank the Department of Earth Sciences, University of Oxford, for financial support for two field seasons to undertake palaeomagnetic sampling. We also thank Gerald Roberts, Birbeck College (University of London), who provided generous financial support for parts of this study.

References

- Allen, P.A. 2008. From landscapes into geological history. *Nature*, **451**, 274–276.
- Barnolas, A. and Teixell, A. 1994. Platform sedimentation and collapse in a carbonate-dominated margin of a foreland basin (Jaca basin, Eocene, southern Pyrenees). *Geology*, **22**, 1107–1110.
- Barnolas, A. and Gil-Peña, I. 2001. Ejemplos de relleno sedimentario multi episódico en una cuenca de antepaís fragmentada: La Cuenca Surpirenaica. *Boletín Geológico y Minero de España*, **112**, 17–38.
- Barnolas, A., Samsó, J.M., Teixell, A., Tosquella, J.Y. and Zamorano, M. 1991. Evolución sedimentaria entre la cuenca de Graus-Tremp y la cuenca de Jaca-Pamplona. I Congreso del Grupo Español del Terciario, Libro Guía de la excursión n°1, EUMO Gràfic, Vic, 123.
- Bayliss, N.J. and Pickering, K.T. 2015a. Transition from deep-marine lower-slope erosional channels to proximal basin-floor stacked channel-levée-overbank deposits, and syn-sedimentary growth structures, Middle Eocene Banastón System, Aínsa Basin, Spanish Pyrenees. *Earth-Science Reviews*, **144**, 23–46.
- Bayliss, N.J. and Pickering, K.T. 2015b. Deep-marine structurally confined channelised sandy fans: middle Eocene Morillo System, Aínsa Basin, Spanish Pyrenees. *Earth-Science Reviews*, **144**, 47–81.

Bentham, P. 1992. *The tectono-stratigraphic development of the western oblique ramp of the South-Central Pyrenean thrust system, northern Spain*. PhD Thesis, 253 pp., University of Southern California.

Bentham, P.A. and Burbank, D.W. 1996. Chronology of Eocene foreland basin evolution along the western margin of the South-Central Pyrenees. In: Friend, P.F. and Dabrio, C.J. (eds), *Tertiary basins of Spain, the stratigraphic record of crustal kinematics*, 144–152. Cambridge University Press, Cambridge.

Bown, P.R. and Young, J.R. (1998) Techniques. In: Bown, P.R., Ed., *Calcareous Nannofossil Biostratigraphy* (British Micropalaeontological Society Publications Series), Chapman and Kluwer Academic, London, 16–28.

Caja, M.A., Marfil, R., García, D., Remacha, E., Morad, S., Mansurbeg, H., Amorosi, A., Martínez-Calvo, C. and Lahoz-Beltrá, R. 2010. Provenance of siliciclastic and hybrid turbiditic arenites of the Eocene Hecho Group, Spanish Pyrenees: implications for the tectonic evolution of a foreland basin. *Basin Research*, **22**, 157–180.

Cantalejo, B., Pickering, K.T., Miller, K.G. and McNiocaill, C. (in review) Chasing the 400-kyr pacing of deep-marine sandbodies: Middle Eocene Ainsa Basin, Spanish Pyrenees. *Journal of the Geological Society*, in review.

Cantalejo, B. and Pickering K.T. 2015. Orbital forcing as principal driver for fine-grained deep-marine siliciclastic sedimentation, Middle-Eocene Ainsa Basin, Spanish Pyrenees. *Palaeogeography, Palaeoclimatology, Palaeoecology*, **421**, 24–47.

Canudo J.I. and Molina E. 1988. Biocronología de foraminíferos planctónicos de la secuencia deposicional de Jaca (Pirineo Aragonés): Eoceno medio y superior. In: *II Congreso Geológico de España, Granada. Comunicaciones*, **1**, 273–276.

Castelltort, S., Honegger, L., Adatte, T, Clark, J.D., Puigdefàbregas, C., Spangenberg, J.E., Dykstra, M.L. and Fildani, A. 2017. Detecting climatic and tectonic signals with carbon isotopes in deep-marine strata, Eocene Aínsa basin, Spanish Pyrenees. *Geology*, **45**, 707–710.

Cecil, C.B. 2003. The concept of autocyclic and allocyclic controls on sedimentation and stratigraphy, emphasizing the climatic variable. *Journal of Sedimentary Research, Special Publication*, **77**, 13–20.

Clark, J., Puigdefabregas, C., Castelltort, S. and Fildani, A. (compilers and editors) 2017. *Propagation of Environmental signals within source to sink stratigraphy*. SEPM Field Trip Guidebook No. **13**: Tulsa Oklahoma, 63 pp.

Costa, E., Garcés, M., López-Blanco, M., Serra-Kiel, J., Bernaola, G., Cabrera, L. and Beamud, E. 2013. The Bartonian-Priabonian marine record of the eastern South Pyrenean Foreland Basin (NE Spain): A new calibration of the larger foraminifers and calcareous nannofossil biozonation. *Geologica Acta*, **11**, 177–193.

Cuevas-Gonzalo, M.C. 1989. *Sedimentary facies and sequential architecture of tide-influenced 656 alluvial deposits. An example from the middle Eocene Capella Formation, South-Central Pyrenees, Spain*. PhD thesis, University of Utrecht.

Das Gupta, K. 2008. *Tectono-stratigraphic evolution of deep-marine clastic systems in the Eocene Aínsa and Jaca basins, Spanish Pyrenees: petrographic and geochemical constraints*. PhD Thesis, University College London, 236 pp.

Das Gupta, K. and Pickering, K.T. 2008. Petrography and temporal changes in petrofacies of deep-marine Aínsa-Jaca basin sandstone systems, Early and Middle Eocene, Spanish Pyrenees. *Sedimentology*, **55**, 1083–1114.

De Federico, A. 1981. La sedimentación de talud en el sector occidental de la cuenca paleógena de Aínsa. PhD Thesis. Universidad Autónoma de Barcelona, *Publicaciones de Geología*, **12**, 271–272.

Dreyer, T., Corregidor, J., Arbués, P and Puigdefábregas, C. 1999. Architecture of the tectonically influenced Sobrarbe deltaic complex in the Aínsa Basin, northern Spain. *Sedimentary Geology*, **127**, 127–169.

Elverhøi, A., Norem, H., Andersen, E.S., Dowdeswell, J.A., Fossen, I., Haflidason, H., Kenyon, N.H., Laberg, J.S., King, E.L., Sejrup, H.P., Solheim, A. and Vorren, T. 1997. On the origin and flow behavior of submarine slides on deep-sea fans along the Norwegian–Barents Sea continental margin. *Geo-Marine Letters*, **17**, 119–125.

Farrell, S.G., Williams, G.D. and Atkinson, C.D. 1987. Constraints on the age of movement of the Montsec and Cotiella thrusts, south central Pyrenees, Spain. *Journal of the Geological Society of London*, **144**, 907–914.

- Fernández, O., Muñoz, J.A., Arbués, P., Falivene, O. and Marzo, M. 2004. 3-D reconstruction of geological surfaces: an example of growth strata and turbidite systems from the Aínsa basin (Pyrenees, Spain). *American Association of Petroleum Geologists Bulletin*, **88**, 1049–1068.
- Fernández, O., Muñoz, J.A., Arbués, P. and Falivene, O. 2012. 3D structure and evolution of an oblique system of relaying folds: the Aínsa basin (Spanish Pyrenees). *Journal of the Geological Society London*, **169**, 545–559.
- Gradstein, F.M., Ogg, J.G. and Schmitz, M. 2012. *The Geological Time Scale 2012*. Amsterdam: Elsevier Science & Technology Books, 1144 pp.
- Holl, J.E. and Anastasio, D.J. 1993. Paleomagnetically derived folding rates, southern Pyrenees, Spain. *Geology*, **21**, 271–274.
- Labauve, P., Séguret, M. and Seyve, C. 1985. Evolution of a turbiditic foreland basin and analogy with an accretionary prism: Example of the Eocene South-Pyrenean basin. *Tectonics*, **4**, 661–685.
- López-Blanco, M., Marzo, M. and Muñoz, J.A. 2003. Low-amplitude, synsedimentary folding of a deltaic complex: Roda sandstone (lower Eocene), South-Pyrenean Foreland Basin. *Basin Research*, **15**, 73–95.
- Lurcock, P.C. and Wilson, G.S. 2012. PuffinPlot: A versatile, user-friendly program for paleomagnetic analysis. *Geochemistry, Geophysics, Geosystems*, **13**, 1–6.
- Martini, E. 1971. Standard Tertiary and Quaternary calcareous nannoplankton zonation. In: A. Farinacci (ed.). Proceedings of the Second International Conference on Planktonic *Microfossils*, **2**, 739–785.
- Marzo, M., Nijman, W. and Puigdefábregas, C. 1988. Architecture of the Castissent fluvial sheet sandstones, Eocene, South Pyrenees, Spain. *Sedimentology*, **35**, 719–738.
- Matenco, L.C. and Haq, B.U. 2020. Multi-scale depositional successions in tectonic settings. *Earth-Sciences Review*, **200**, 102991.
- Miller, K.G., Wright, J.D. and Browning, J. 2005. Visions of ice sheets in a greenhouse world. *Marine Geology*, **217**, 215–231.

- Millington, J.J. and Clark, J.D. 1995. The Charo/Arro canyon-mouth sheet system, south-central Pyrenees, Spain: a structurally influenced zone of sediment dispersal. *Journal of Sedimentary Research*, **65**, 443–454.
- Mochales, T., Barnolas, A., Pueyo, E.L., Serra-Kiel, J., Casas, A.M., Samsó, J.M., Ramajo, J. and Sanjuan, J. 2012a. Chronostratigraphy of the Boltaña anticline and the Aínsa basin (Southern Pyrenees). *Bulletin of the Geological Society of America*, **124**, 1229–1250.
- Mochales, T., Casas, A.M., Pueyo, E.L. and Barnolas, A. 2012b. Rotational velocity for oblique structures (Boltaña anticline, Southern Pyrenees). *Journal of Structural Geology*, **35**, 2–16.
- Mochales, T. 2010. *Chronostratigraphy, vertical axis rotations and AMS in the Boltaña anticline (Southern Pyrenees): kinematic implications*. PhD Thesis, University of Zaragoza (Spain).
- Muñoz, J.A. 1992. Evolution of a continental collision belt: ECORS-Pyrenees crustal balanced cross-section. In: McClay, K.R. (ed.), *Thrust Tectonics*, 235–246. Chapman & Hall, New York.
- Muñoz, J.A., McClay, K. and Poblet, J. 1994. Synchronous extension and contraction in frontal thrust sheets of the Spanish Pyrenees. *Geology*, **22**, 921–924.
- Muñoz, J.A., Arbués, P. and Serra-Kiel, J. 1998. The Aínsa basin and the Sobrarbe oblique thrust system: Sedimentological and tectonic processes controlling slope and platform sequences deposited synchronously with a submarine emergent thrust system. In: Meléndez Hevia, A. & Soria, A.R. (eds), *Field Trip Guidebook of the 15th International Association of Sedimentologists International Congress of Sedimentology*, 213–223.
- Muñoz, J.A., Beamud, E., Fernández, O., Arbués, P., Dinarès-Turell, J. and Poblet, J. 2013. The Aínsa fold and thrust oblique zone of the central Pyrenees: kinematics of a curved contractional system from paleomagnetic and structural data. *Tectonics*, **32**, 1142–1175.
- Mutti, E., Luterbacher, H.P., Ferrer, J. and Rosell, J. 1972. Schema stratigrafico e lineamenti di facies del Paleogene marino della zona central subpirenaica tra Tremp (Catalogna) e Pamplona (Navarra). *Societa Geologica Italiana*, **11**, 391–416.
- Mutti, E., Remacha, E., Sgavetti, M., Rosell, J., Valloni, R. and Zamorano, M. 1985. Stratigraphy and facies characteristics of the Eocene Hecho Group turbidite systems, south-central Pyrenees. In: Mila, M.D. and Rosell, J. (eds), *Excursion Guidebook of the 6th*

European Regional Meeting of International Association of Sedimentologists, Lerida, 233–291.

Mutti, E, Séguret, M and Sgavetti, M. 1988. Sedimentation and deformation in the Tertiary sequences of the southern Pyrenees. Fieldtrip 7 Guidebook. *American Association of Petroleum Geologists*, Mediterranean Basins Conference, Nice, France, 153–157. Special Publication of the Institute of Geology of the University of Parma.

Nannotax3 - Young, J.R., Bown P.R. and Lees J.A. (eds). Nannotax website. International Nannoplankton Association. URL: <http://www.mikrotax.org/Nannotax3/>.

Nijman, W. 1998. Cyclicity and basin axis shift in a piggyback basin: towards modelling of the Tremp-Ager Basin, South Pyrenees, Spain. *In*: Mascle, A., Puigdefabregas, C., Luterbacher, H.P. and Fernández, M. (eds) *Cenozoic Foreland Basins of Western Europe. Geological Society Special Publication*, **134**, 135–162.

Oms, R., Dinares-Turell, J. and Remacha, E. 2003. Magnetic stratigraphy from deep clastic turbidites: an example from the Eocene Hecho Group (southern Pyrenees). *Studies in Geophysics and Geodynamics*, **47**, 275–288.

Payros, A., Tosquella, J., Bernaola, G., Dinares-Turell, J., Orue-Etxebarria, X. and Pujalte, V. 2009. Filling the North European Early/Middle Eocene (Ypresian/ Lutetian) boundary gap: Insights from the Pyrenean continental to deep-marine record. *Palaeogeography, Palaeoclimatology, Palaeoecology*, **280**, 313–332.

Payros, A., Pujalte, V. and Orue-Etxebarria, X. 1999. The South Pyrenean Eocene carbonate megabreccias revisited: new interpretation based on evidence from the Pamplona Basin. *Sedimentary Geology*, **125**, 165–194.

Pickering, K.T. and Bayliss, N.J. 2009. Deconvolving tectono-climatic signals in deep-marine siliciclastics, Eocene Aínsa basin, Spanish Pyrenees: Seesaw tectonics versus eustasy. *Geology*, **37**, 203–206.

Pickering, K.T. and Corregidor, 2000. 3D reservoir-scale study of Eocene confined submarine fans, south-central Pyrenees. *In*: Weimer, P., Slatt, R.M., Coleman, J., Rosen, N.C., Nelson, H., Bouma, A.H., Styzen, M.J. and Lawrence, D.T. (eds), *Deep Water Reservoirs of the World*, 776–781. Gulf Coast Section, Society of Economic Palaeontologists

and Mineralogists, Foundation 20th Annual Bob F. Perkins Research Conference, Houston, Texas.

Pickering, K.T. and Corregidor, J. 2005. Mass-Transport Complexes (MTCs) and tectonic control on basin-floor submarine fans, Middle Eocene, South Spanish Pyrenees. *Journal of Sedimentary Research*, **75**, 761–783.

Pickering, K.T., Corregidor, J. and Clark, J. 2015. Architecture and stacking patterns of lower-slope and proximal basin-floor channelized submarine fans, Middle Eocene Aínsa system, Spanish Pyrenees: an integrated outcrop-subsurface study. *Earth-Science Reviews*, **144**, 47–81.

Pickering, K.T. and Cantalejo, B. 2015. Deep-marine environments of the Middle Eocene Upper Hecho Group, Spanish Pyrenees: Introduction. *Earth-Science Reviews*, **144**, 1–9.

Pickering, K.T. and Hiscott, R.N. (with contribution by Heard, T.G.) 2016. Deep Marine Systems: Processes, Deposits, Environments, Tectonic and Sedimentation. Wiley and American Geophysical Union (AGU), 672 pp. ISBN: 978-1-4051-2578-9.

Poblet, J., Muñoz, J.A., Travé, A. and Serra Kiel, J. 1998. Quantifying the kinematics of detachment folds using three-dimensional geometry: application to the Mediano anticline (Pyrenees, Spain). *Geological Society of America Bulletin*, **110**, 111–125.

Poyatos-Moré, M. 2014. Physical Stratigraphy and Facies Analysis of the Castissent Tecto-Sedimentary Unit (South Central Pyrenees, Spain): Depositional processes and controlling factors of sediment dispersal from river-mouth to base-of-slope settings. PhD Thesis, Universitat Autònoma de Barcelona, 291 pp. <http://hdl.handle.net/10803/145397>

Puigdefábregas, C. 1975. La sedimentación molásica en la cuenca de Jaca. *Pirineos*, **104**, 1–188.

Puigdefábregas, C., Muñoz, J.A. and Vergés, J. 1992. Thrusting and foreland basin evolution in the Southern Pyrenees. In: McClay, K.R. (ed.), *Thrust Tectonics*, 247–254. Chapman and Hall.

Remacha, E., Fernandez, L.P., Maestro, E., Oms, O. and Estrada, R. (with a contribution by Teixell, A.) 1998. Excursion A1. The Upper Hecho Group turbidites and their vertical evolution to deltas (Eocene, South-central Pyrenees). International Association of

Sedimentologists, 15th International Sedimentological Congress, Alicante, Spain, Field Trip Guidebook, 1–25.

Remacha, E., Oms, O. and Coello, J. 1995. The Rapitán turbidite channel and its related eastern levée-overbank deposits, Eocene Hecho group, south-central Pyrenees, Spain. *In*: Pickering, K.T., Hiscott, R.N., Kenyon, N.H., Ricci Lucchi, F. and Smith, R.D.A. (eds), *Atlas of Deep Water Environments: Architectural Style in Turbidite Systems*, 145–149. Chapman & Hall, London.

Remacha, E., Gual, G., Bolaño, F., Arcuri, M., Oms, O., Climent, F., Crumeyrolle, P., Fernández, L.P., Vicente, J.C. and Suárez, J. 2003. Sand-rich turbidite systems of the Hecho Group from slope to the basin plain: facies, stacking patterns, controlling factors and diagnostic features: *American Association of Petroleum Geologists*, International Conference and Exhibition, Barcelona, Spain, September 21–24. Geological Field Trip no. 12, South-Central Pyrenees.

Remacha, E. & Fernández, L.P. 2003. High-resolution correlation patterns in the turbidite systems of the Hecho Group (South-Central Pyrenees, Spain). *Marine and Petroleum Geology*, **20**, 711–726.

Rodríguez-Pintó, A., Pueyo, E.L., Serra-Kiel, J., Samsó, J.M., Barnolas, A. and Pocoví, A. 2012. Lutetian magnetostratigraphic calibration of larger foraminifera zonation (SBZ) in the Southern Pyrenees: The Isuela section. *Palaeogeography, Palaeoclimatology, Palaeoecology*, **333–334**, 107–120.

Romans, B.W.; Castelltort, S., Covault, J.A., Fildani, A. and Walsh, J.P. 2016. Environmental signal propagation in sedimentary systems across timescales. *Earth-Science Reviews*, **153**, 7–29.

Scotchman, J.I., Bown, P., Pickering, K.T., BouDagher-Fadel, M., Bayliss, N.J. and Robinson, S.A. 2015. A new age model for the middle Eocene deep-marine Aínsa Basin, Spanish Pyrenees. *Earth-Science Reviews*, **144**, 10–22.

Serra-Kiel, J., Canudo, J.I., Dinarès, J., Molina, E., Ortiz, N., Pascual, J.O., Samsó, J.M. and Tosquella, J. 1994. Cronoestratigrafía de los sedimentos marinos del terciario inferior de la

cuena de Graus-Tremp (Zona Central Surpirenaica). *Revista de la Sociedad Geológica de España*, **7**, 273–297.

Sutcliffe, C. and Pickering, K.T. 2009. End-signature of deep-marine basin-fill, as a structurally confined low-gradient clastic slope: the Middle Eocene Guaso system, south-central Spanish Pyrenees. *Sedimentology*, **56**, 1670–1689.

Teixell, A. 1996. The Ansó transect of the southern Pyrenees: basement and cover thrust geometries. *Journal of the Geological Society*, **153**, 301–310.

Torsvik, T.H., Briden, J.C. and Smethurst, M.A. 2000. Super-IAPD Interactive analysis of paleomagnetic data. Downloaded from: www.geodynamics.no/software.htm (13/1/2016).

Tosquella, J. 1995. *Els Nummulitinae del Paleocè-Eocè inferior de la conca sudpirinenca*. Ph.D. thesis, University of Barcelona, Barcelona, Spain, 581 pp.

Van Lunsen, H.A. 1970. *Geology of the Ara-Cinca Region, Spanish Pyrenees, Province of Huesca*. PhD Thesis, Utrecht University.

Vergés, J., Fernández, M. and Martínez, A. 2002. The Pyrenean orogen; pre-, syn-, and postcollisional evolution. *Journal of the Virtual Explorer*, **8**, 57–76.

Westerhold, T., Röhl, U., Donner, B., Frederichs, T., Kordesch, W.E.C., Bohaty, S.M., Hodell, D.A., Laskar, J. and Zeebe, R.E. 2018. Late Lutetian Thermal Maximum – crossing a thermal threshold in Earth's climate system? *Geochemistry, Geophysics, Geosystems*, **19**, 73–82.

Figure captions

Supplementary materials

Supplementary material 1. Field photographs of the sampled sections.

Supplementary material 2. Natural remnant magnetism (NRM) measured on 415 samples of siltstones and very fine-grained sandstone turbidites from the Ainsa Basin.

Supplementary material 3. Species range charts used in this study. Taxonomy follows Nannotax (<http://www.mikrotax.org/Nannotax3>).

Supplementary material 4. Alternative age-model scenario, with shift of the identified magnetic reversals to a younger part of the stratigraphy. The R1-N1; N1-R2 and R2-N2 reversals become the C20r/C20n, C20n/C19r and C19r–C19n, respectively. This produces a significant time offset with our key nannofossils markers and is, therefore, problematic.

Supplementary material 5. Multiple stacked MTDs around the village of Castellazo (**A**), and in the Rio Sieste (Morillo System) (**B**), cited by Clark et al. (2017) as key locations for correlating the so-called megaturbidite "MT-4" (MTD or MTDs following the terminology in Pickering and Hiscott, 2016) from the Jaca to Aínsa basins.